PHYSICAL MODELS DESIGNED FOR VASCULAR STENOSIS AND FLUID DYNAMIC STUDIES

by

MONICA MICHELLE RODAS

A thesis submitted to the

Graduate School-New Brunswick

Rutgers, The State University of New Jersey

And The Graduate School of Biomedical Sciences

University of Medicine and Dentistry of New Jersey

In partial fulfillment of the requirements

For the degree of

Master of Science

Graduate Program in Biomedical Engineering

Written under the direction of

Dr. Gary Drzewiecki, Ph.D

And approved by

_____

_____

_____

New Brunswick, New Jersey

May 2012

ABSTRACT OF THE THESIS

PHYSICAL MODELS DESIGNED FOR VASCULAR STENOSIS AND FLUID DYNAMIC STUDIES

By MONICA MICHELLE RODAS

Thesis Director:

Dr. Gary Drzewiecki, Ph.D

Atherosclerosis and Cardiovascular disease make up the leading cause of death in the United States. The disease occurs when plaque develops on lesions in the arterial lumen causing narrowing and hardening of the vessel walls. When the lumen cross-sectional area continues to decrease, the velocity of blood increases eventually becoming turbulent. This blood flow turbulence is believed to produce a sound in the occluded artery known as a bruit. Carotid auscultations are considered the golden standard for stenosis screening. However, recent studies suggest this is a poor predictor of carotid stenosis (sensitivity: 11% -51%). There are inaccuracies in relationships between vascular bruits and severity of the disease. Bruits can be missed due to loud sounds produced in the arteries and may be out of the range of human hearing. Therefore, an understanding of the fluid dynamics of diseased arteries will provide more accurate noninvasive methods for detecting and classifying arterial stenosis.

This thesis proposes that physical models may be used to simulate the fluid dynamics of the diseased artery. In this research, experiments were conducted on three

physical models that represent different geometries of stenosis. The models consisted of latex tubing with a bending modulus and cross-sectional area similar to a carotid artery in situ. A constant mean flow was passed through the lumen of the models, and the wall displacements and sounds produced were obtained and analyzed. The recording devices consisted of a piezoelectric material, optical sensor, and electronic stethoscope. The results show that stenosis facing a flexible wall produces greater wall vibrations than a symmetrical rigid stenosis. It was found that increasing the length of a plaque dome results in higher frequencies. The Continuous Wavelet Transforms (CWTs) of the measurements showed that stenosis with rigid symmetry reduces the amount of wall motion and sounds produced in time. The models have shown that wall motion is affected by stenotic geometries and thus provides a useful approach to the study of fluid dynamics of vascular disease. These relationships can be used to increase the sensitivity of classifying and detecting the structure of stenosis using noninvasive devices.

Acknowledgements

First and foremost, I would like to thank my thesis director, Dr. Gary Drzewiecki, who has supported me throughout my research. His patience and mentorship has provided me with exceptional knowledge and experience with biomedical research. I am grateful for his effort in helping me solve technical issues in the lab, educating me, wisely guiding my input, and editing my thesis. I have found that doing research with him has been fun, intellectually rewarding, and has developed my skills to a great extent. It has truly been a pleasure working under his advisement and without him this thesis would not be possible.

I thank my committee members, Dr. John K-J. Li and Dr. William Craelius, for participating in my Masters thesis defense. It was a privilege to discuss and answer questions regarding my research and having them share their expertise with me.

The department of Biomedical Engineering at Rutgers University has provided me with access to the laboratory and equipment to conduct my research.

If it were not for my fellow graduate student and best friend that I have made at Rutgers University, Dmitry (Dima) Khavulya, I would not have matured as quickly as I did during my education. I thank him for making a true college experience for me. One could not ask for a better friend.

I would like to thank my close friends and companions, Dmitry Miretskiy, Keith Govert, and Randy Hunter, for making my social life fun, exciting, and interesting.

Finally, I would like to thank my parents immensely for inspiring me to pursue a Masters degree in Biomedical Engineering and supporting me financially. Completing a

Masters degree in Biomedical Engineering has been encouraged and supported daily by my loving family. From a very young age, my parents, Carlos Alejandro Rodas and Bertha Maria Rodas, have taught me the importance of higher education. I thank my brother, Alejandro Daniel (Danny) Rodas, for always being there for me. I thank my extended family, my uncle, William Rodas, and my cousin, Maria (Mima) Estrabao, for their help throughout my education.

Dedication

This thesis is dedicated to my loving and supportive family.

In loving memory of my grandfather, Jose Miguel Miranda.

Table of Contents

List of Tables

List of Figures

Chapter 1

Introduction

Carotid stenosis is the build up of plaque on the carotid artery, which causes the blockage of blood flow by continued narrowing of the carotid artery. The disease in general is known as Atherosclerosis, and it can occur in other arteries. Currently, Cardiovascular (CVD) disease and Atherosclerosis is the leading cause of death in the United States affecting 82.6 million Americans in 2008 [1], [2], [15]. The carotid artery is the main artery that supplies oxygen to the brain. Therefore, the formation of carotid stenosis is a major risk factor for cerebrovascular events due to oxygen deprivation from reduced blood flow. Cerebrovascular events such as: cerebral embolism, transient ischemic attack (TIA) and stroke may occur, which can lead to temporary or permanent brain damage or even death. According to the American Heart Association (AHA), in 2008, 7 million Americans suffered a stroke, with approximately 795 thousand experiencing a new or recurrent stroke [15]. The total costs of treating CVD are increasing due to the greater number of cases of CVD in succeeding years. There was a total of 27% increase in inpatient cardiovascular surgery and procedures from 1997 to 2007 [15]. It costs more than any other diagnostic group to treat; $228 billion in 2008 [15].

1.1 Prior data on bruits:

A physician will suspect carotid stenosis if a patient has one of the following symptoms, high blood pressure, syncope, stroke, TIA or presence of a bruit [16]. These symptoms typically are indications of late stages of the disease. According to the

Vascular Disease Foundation, there are usually no advance warnings related to the early stages of carotid stenosis, except a TIA [17]. The golden standard however for screening for carotid stenosis is auscultations of the artery with a standard stethoscope [10]. During auscultations of the carotid artery, the physician will search for a bruit. A bruit is a whooshing sound produced in severely occluded arteries [6], [8], [9]. This sound is believed to be produced by high velocities that cause turbulent flow, which is characterized by a Reynold's number greater than 5000 [6], [14]. The problem with carotid auscultations is that it relies on the physician's judgment of the sounds produced in the artery, which leaves room for a lot of human error. Some studies suggest this is a poor predictor of carotid stenosis [8]. One study even claims finding bruits in subjects without stenosis [9]. Another reason why bruits may be misinterpreted or missed is because the artery tends to be naturally noisy due to the blood flowing through them or they are out of the range of human hearing [10]. Understanding about the mechanical behavior of diseased vessels is needed to contribute to more effective measures of stenosis.

Carotid bruits have been studied, but show inconsistencies in results. These variability's in results indicate the need for further studies from a mechanical modeling perspective to better understand the nature of the bruits. Dr. Tavel, has studied carotid bruits in many patients using Doppler-ultrasound. Dr. Tavel has found that later stages of stenosis produce sounds with higher frequency ranges and for a longer duration in time [6]. Even in Tavel's findings, the study consisted of 80 patients, but only 76 patients had satisfactory sound recording. The relationships between severity of disease and duration and frequencies of bruit were found on 58% of the recordings. In this paper, Dr. Tavel

also points out that accuracies depend on the expertise of a laboratory. Tavel mentions that sound spectral analysis performed on an outside laboratory resulted in a mild degree diagnosis of stenosis, but in his lab it was found to be a high grade stenosis. There are also inconsistencies with the frequency range that bruits occur. Dr. Tavel mentions that for higher grade stenosis, bruits occur at a range greater than 300 Hz. This leaves room for a lot of interpretation because he doesn't really mention frequency ranges. In one study by Miller, conducted to measure bruits produced on an in vivo study of carotid arteries of dogs, the bruits occurred in a broad range of frequencies from 100-1500 Hz [35]. In this study, the researchers attempted to show that surrounding tissues dampen wall vibrations. They did this by creating a surgical incision to expose the carotid artery of a dog and applying a Teflon band around the carotid artery. Recordings were done to measure vibrations produced on the carotid artery while it was exposed and after wound healed. Although, the study did find that external tissues dampen the wall vibrations (100-800 Hz), the sound spectra was still obtained and showed that resistance around the vessel does cause vibrations and are related to the sounds produced. The stenosis produced in Miller's experiment is similar to the rigid model designed in this research. This research however, also studies the mechanical behaviors of other possible stenosis geometries. In this research, the plaque dome geometries are similar to those found in MRI images shown in Sikdar's study [34]. Sikdar showed vibrations occurring in the vessel, but with the geometries similar to the plaque dome model, he was able to find vibrations through the tissue occurring in the 23-1500 Hz frequency range. Sikdar found that as this asymmetrical geometry becomes more severely occluded that higher frequency vibrations occur. Miller's symmetrical stenosis and Sikdar's clinical studies

on asymmetrical stenosis with ranges of severity support the overall results found in this research. The previous studies indicate that stenosis produced vibrations, but the vibrations occurring in symmetrical stenosis are more damped than asymmetrical stenosis. A similar relationship is found in the physical models used in this research, which can be used with further experiments to find other facts about the disease.

1.2 Artery Anatomy and Physiology and Disease Morphology:

Arterial walls are composed of three embedded layers, the tunica intima, tunica media, and the adventitia [13]. The tunica intima is the inner most layer in the vessel which consists of a thin layer of endothelial cells, connective tissue and basement membrane [13], [20]. This layer is the innermost layer of the arterial wall and it is in direct contact with the blood in the arterial lumen. It is in this layer that artherosclerosis begins to develop. The endothelial tissue in this layer allows for a smooth and friction reducing lining. The tunica media, is the layer inbetween the tunica intima and the adventitia. This layer consists of smooth muscle cells and a continuous layer of interstitial fluid of proteoglycan and collagen fibers [13],[20]. The smooth muscle cells are responsible for contraction and relaxation of the artery, whereas the elastin allows the artery to coil and recoil. The outer most layer, the adventitia, is mostly composed of stiff collagen fibers which protects the artery and anchors it to surrounding structures [13]. An illustration of the sub layers in the arterial wall is presented in Figure 1.

Arteries are just one kind of blood vessels (arteries, capillaries and veins) that are part of a closed delivery system that starts and ends at the heart. The arteries function to supply blood from the heart to the rest of the body. Since the arteries are the vessels

closest to the heart, they are subjected to higher pressures and thus have a thicker tunica media.

Atherosclerosis is a chronic arterial disease caused by the accumulation of plaque composed of fats, cholesterol, calcium, and other substances on the inner most layer of the arterial wall [12]. Overtime, these deposits on the endothelium of the inner walls of the arteries cause the arteries to harden and thicken, and thus reducing its elasticity.

The precise mechanism of atherosclerosis is not well understood. Some evidence however, has showed that fatty streaks can begin to accumulate in the arterial wall as early as childhood [12]. Low Density Proteins (LDLs), known as "bad cholesterol," are proteins that carry cholesterol to the body. When fatty deposits, primarily LDLs, accumulate in the lining of the epithelial tissues, immune cells called macrophages begin to ingest these materials. When these macrophages become filled with lipids they are known as "foam cells." These foam cells eventually die and accumulate in the lining of the arterial walls causing tiny lesions [2]. The lesions develop into scar tissue causing loss of elasticity of the artery, which adds resistance to the artery and resulting in an increase in Blood Pressure and an affect on flow [18]. Equation 1 below describes Ohm's law for fluids, based on the fundamental laws of physics. The relationship between pressure and resistance, explains how an increase in resistance causes an increase in pressure. Where P is pressure, Q is flow, and R is resistance. Equation 2 describes the resistance for a vessel of length l, radius r, and fluid viscosity μ. Therefore, as the cross-sectional area becomes smaller by narrowing of the stenosis, the resistance in

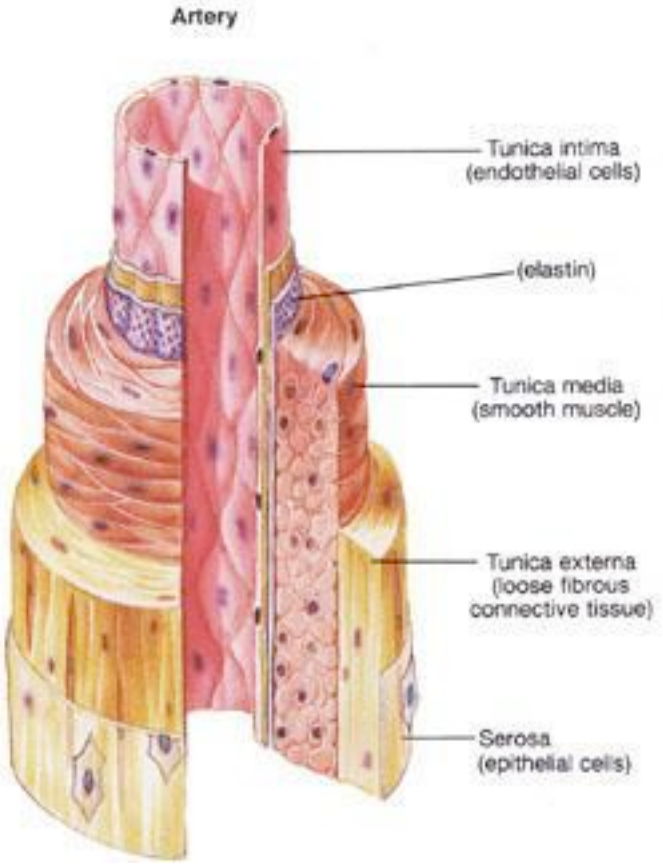

Figure 1: Embedded layers of the arterial wall
(www.stiffarteries.com/arterial-stiffness.php)

the vessel increases and thus the pressure increases. The viscosity in the blood also increases with development of stenosis, as debris and narrowing of the vessel allows for blood clotting, which also increases the resistance, and thus raising pressure.

1. $\Delta P = P_{upstream} - P_{downstream} = Q * R$

2. $R = 8*\mu * l / (\pi * r^4)$

Figure 2 illustrates an example of plaque build up and lesion formation. Overtime, the cross-sectional area will decrease causing a noticeable change in pressure. In the experiments conducted in this research, the models are not pressurized as vessels are in a closed circulatory system, but we are merely analyzing the results by decreasing the order of the pressure. An example of this is illustrated in figure 3. Therefore, the results will be an order lower, but will still explain the mechanics of the disease. The models were purposely experimented with an open system to observe measurements of pressure across the stenosis. In one study conducted by Turk et al, stenosis was generated in the carotid arteries of canines and the pressure gradient across stenosis were in the range of 6-26 mmHg [36]. Similar pressure ranges are found in the models studied in this research. The addition of more fatty deposits on the epithelial lining of the arterial walls can eventually occlude the artery. This will limit blood flow to the heart, brain, and other tissues, potentially causing tissue damage, heart attack and/or stroke.

Several models of obstructed vessels have been developed to describe the abnormal flow patterns of diseased arteries, but the exact mechanism of the disease is not well understood. Modeling of arterial stenosis is necessary to provide information about the disease that can be useful for the development of new technologies that screen for atherosclerosis. Some computational models have been developed to describe the affects

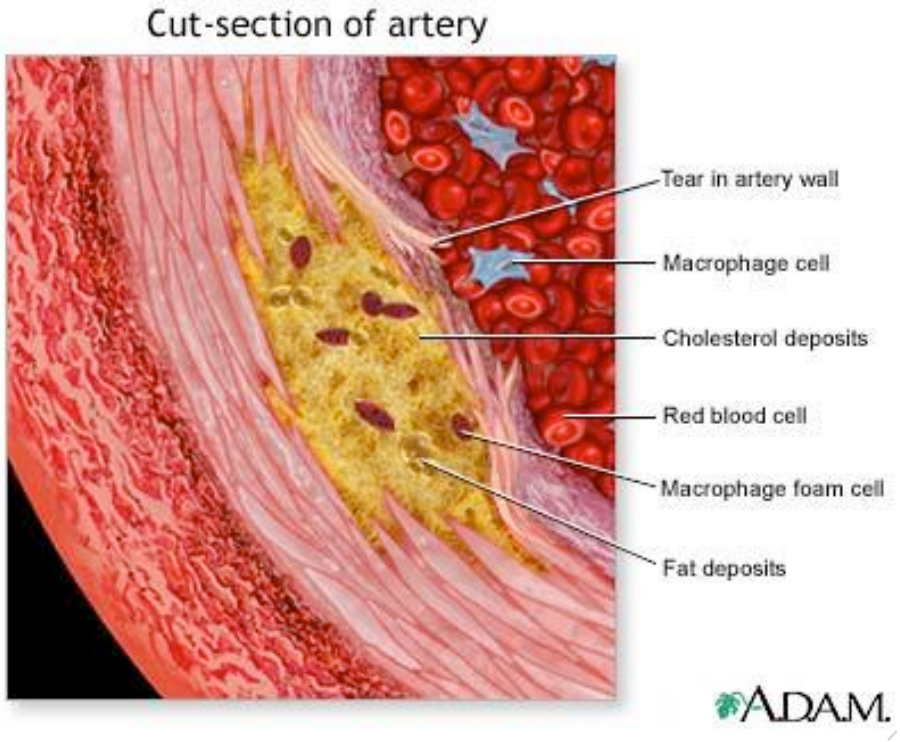

Figure 2: Fatty deposits accumulating on lesion site in the lumen of an artery (www.umm.edu/imagepages/18018.htm)

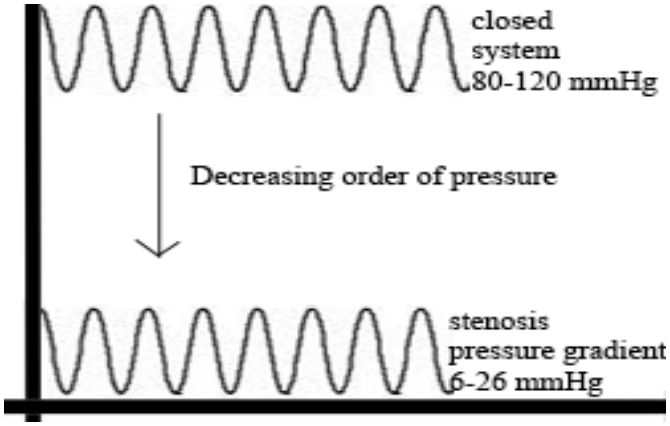

Figure 3: Decreasing order of pressurized diseased vessel

of flow passing through the lumen of the occluded artery [19],[21],[22]. Although this information is useful, flow is usually affected during very late stages of atherosclerosis. This occurs when the cross-sectional area of the lumen has decreased enough to create a jet flow through the narrowed region causing turbulence [6],[14],[23]. Therefore, information regarding the mechanics of the disease can provide new details about the mechanism of the disease. There are several models that have looked at the mechanical behavior of the disease, in terms of shear stress and shear rate across the stenosis [24],[21],[22]. Current vascular disease models include mathematical, computational, and physical models.

1.3 Previous Models:

1.3.1 Mathematical models:

There are mathematical models used to describe the hemodynamics of stenotic arteries, but some, such as Navier-Stokes equations are discussed with fewer details in physiology classes [23]. J.H. Choi et al, state that the subject of Navier-Stokes equation relating to blood flow,

> …is dealt with in rather limited scheme in physiology classes, since equations are difficult to solve analytically with few exceptions…Another reason for limiting the coverage lies in difficulty in finding easy and interesting examples beyond Hegen-Poiseuille's law for quasi-static pressure gradient.[23]

Prior models are designed to calculate flow through the lumen of the artery [30],[20],[23]. These models are valuable to many of the current technologies used today for detecting stenotic arteries. Hagen-Poiseuille's law for quasi-static pressure gradient is common to the basic fundamental physiology course, and states that in a pipe with a circular cross-sectional area, the rate of flow is proportional to the fourth power of the radius in the pipe [23]. In reality, blood pressure varies sinusoidally, therefore, Hagen-Poiseuiile's law only is an approximation of how velocity increases as cross-sectional area varies with the pulse [28]. This aids in diagnosis of CVD by Doppler-ultrasound, Magnetic Resonance Angiographies (MRAs), and angiography that provide information about the flow in a stenotic artery. In all of these methods, a high blood velocity indicates severe narrowing in the occluded artery [add reference].

Human blood is an incompressible non-Newtonian fluid [20]. The Navier Stokes Equation (NSE) is a model based on Newton's law of motion, and has been used to describe flow [23]. Mathematicians are attempting to solve more difficult equations to describe realistic examples of blood flow by incorporating solutions to Bessel functions with Sexl's equation and Hagen-Poiseuille's equation in NSE [23]. In one study, blood flow was formulated as a two-fluid model, with erythrocytes in the core describing a non-Newtonian fluid and plasma on the peripheral of the flow describing a Newtonian fluid [30]. This model was based on studies that showed that there is a peripheral layer of plasma and erythrocytes in the core in blood flow through narrowed arteries [30].

In another complex mathematical model, mathematicians modeled blood flowing through the lumen and poroelastic wall of the coronary artery [20]. This mathematical model considered wall deformation, but only in one cardiac cycle, by using the equations of classical elastodynamics and equations to calculate shear stress [20].

1.3.2 Computational models:

Computational models are complex and depend on mathematical and experimental models to obtain parameters. If enough and accurate information regarding the model is acquired, computational simulations can be very powerful. However, equations describing flow and mechanical wall behavior of an artery are still difficult to solve and explain [23],[29]. Computational simulations are also useful for postulating information of an artery such as wall shear stress that is not manageable through noninvasive detection [21]. In one study, a computational model of a symmetrical diseased artery was used to study cyclic tube compression and collapse, but in terms of some different inlet pressures [29]. This study also observed negative pressure, wall shear stress, and flow recirculation. Negative pressures were also found in the results of the diseased models used in this research. Another study, ran a Computational Fluid Dynamics (CFD) simulation by considering the wall as a two-layer hyperelastic anisotropic material in a symmetrical fluid-structure model [24]. They found that velocity and wall shear stress increases exponentially with stenosis severity. Although, computational models are useful to simulate flow through diseased arteries, CFD models suffer from the fact that the vessel geometry is not constant.

1.3.3 Physical models:

Physically modeling carotid stenosis and using devices to record the

hemodynamics is another approach to obtaining parameters regarding the flow and mechanics of the disease. To follow this method, the physical models should be as similar as possible to a carotid artery in situ to obtain accurate information. Most of these models are designed to simulate circulation in an artery to observe the behavior regarding flow and also wall shear stress. In one research, a flow is passed through a Plexiglas rigid tube to observe areas of recirculation, which are believed to correlate with lesion formation [22]. In this study, the results had a strong correlation with a tested bovine carotid artery. A recent study, used an unspecified tube with a plaque-like material placed on one side of the artery while an ultrasonic probe was used to measure flow reversal, axial velocities in radial direction, and wall shear stress [19].

1.4 Models regarding this thesis:

In this research, the dynamic behavior of the three diseased vessel models was observed. Each model was designed to represent various geometries of atherosclerosis used with a similar bending modulus and lumen cross-sectional area as carotid arteries. This study is unique because the dynamic behavior is determined in terms of the degree of vessel wall vibrations of the physical models. The wall deflection magnitude upstream, on throat, and downstream of stenosis as well as sound magnitudes of the models was considered. The differences in mechanical properties between a plaque dome and rigid model can describe the mechanism of disease progression. The plaque dome models showed vessel wall vibrations, which were not prominent in the rigid model. This characteristic behavior of distinct geometries of atherosclerosis can be measured using a piezoelectric material. If a medical device is developed to capture wall

vibrations of early stages of carotid stenosis, the costs of treating CVD will decrease and the amount of strokes occurring will also decrease.

Chapter 2

Methods

Modeling blood flow and vessel mechanics of arteries is crucial for Cardiovascular Disease (CVD) research. Data regarding early stages of atherosclerosis is not readily available and since arteries are internal, noninvasive measures of mechanical properties of the vessel is difficult to accomplish. Therefore, biomedical engineers attempt to model the artery in order to extract useful information about the disease. In this chapter, the design of the diseased vessel models, calibration of the devices used, and experimental protocols are discussed.

2.1 Geometry of Diseased Vessel Models

In this research, three models were designed to represent plaque dome and rigid stages of diseased carotid arteries. During plaque development in carotid arteries, fatty debris attaches onto lesions on one side of the epithelial lumen of the artery, leaving a flexible wall on the opposite side. Eventually a fibrous plaque develops on one side of the vessel as seen in Figure 4. In the late stages of carotid stenosis, the fibrous plaque surrounds the site of stenosis symmetrically, creating a rigid cross-sectional area, as seen in Figure 5.

2.1.1 The Rigid Model (RM)

The rigid model in this research represents wall thickening and calcification in the symmetrical narrowed region of stenosis, which occurs in very late stages of atherosclerosis. A piece of hard tubing with an outer diameter the same as the vessel and a smaller inner diameter is placed inside the latex tubing. This model is similar to prior

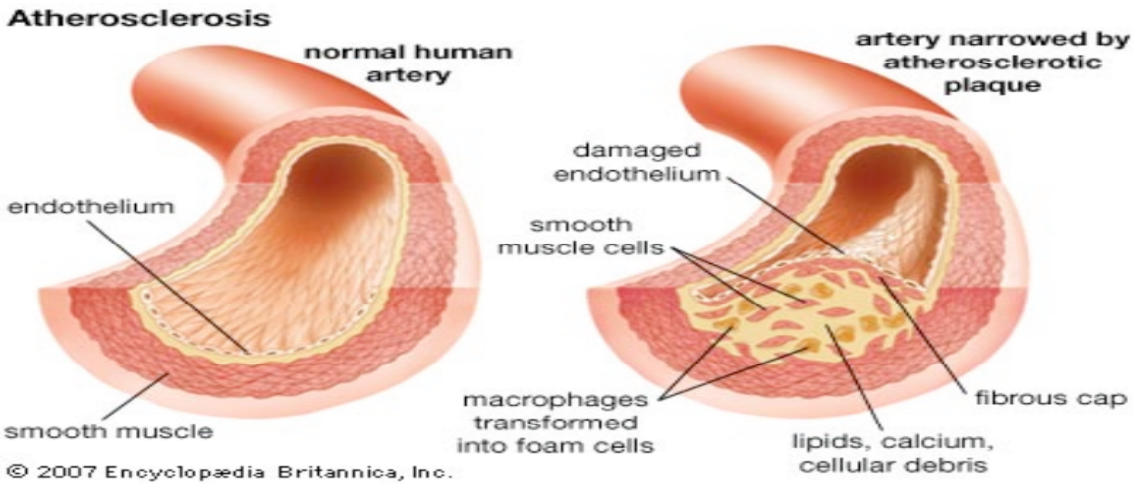

Figure 4: Comparison of a healthy artery (left) and early formation of disease (right). Early stages show plaque dome growing in the inner wall. (www.robertsfox.com/EndoPAT.htm)

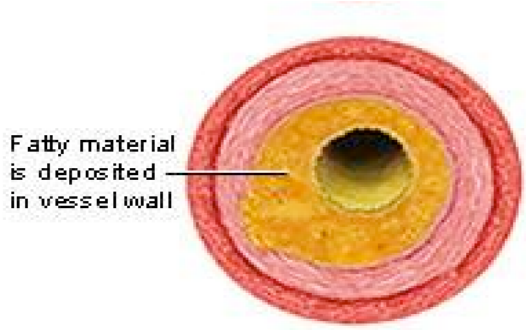

Figure 5: Cross-sectional area of a fully occluded artery; example of late stages of atherosclerosis (http://www.ncbi.nlm.nih.gov/pubmedhealth/PMH0001224/figure/A000171.B18020/?report=objectonly)

models used to describe diseased arteries with a symmetrical narrowing across the stenosis [21-25]. Perhaps other studies have focused on this model because it is more likely that the narrowing stage is associated with cardiovascular events like heart attack, stroke, and clotting. Figure 6 shows the cross-sectional area of this model.

Figure 6: Cross-sectional area of the rigid model. This Model represents complete symmetrical rigidity of the vessel wall.

2.1.2 The Plaque Dome Models (PDM)

Two plaque dome models were created. PDMs with two different lengths of stenosis were designed to observe the relationship between length of stenosis and mechanical properties. The PDM with the shorter length of stenosis is named the short plaque dome model (SPDM) and the other with the longer length is named the long plaque dome model (LPDM). The plaque dome models represent assymetrical stenosis with partial hardening of the walls, which occurs in earlier stages of vascular disease. This model is designed to represent a rigid plaque dome formation on one side of the vessel and therefore a remaining flexible wall on the other side of the plaque dome. The plaque dome was designed by folding one part of the vessel wall inward. Then the folding is glued with cyanoacrylate to hold the plaque dome in place. The cross-sectional areas of

the models used in this research are similar to the cross-sectional areas from the early and late stages of atherosclerosis shown in Figure 4 and 5. In Figure 7, the cross-sectional area of the plaque dome models is shown.

Figure 7: Cross-sectional area of the plaque dome models representing a plaque dome formed on the upper wall and a remaining lower flexible wall.

It can be seen from figure 7, that the lumen of the plaque dome models are not circular. Therefore, deriving flow or mechanical wall behaviors with this model is much more difficult to calculate. However, early stages of atherosclerosis exhibit these characteristics, and thus analysis from a hemodynamic model of early diseased vessels will provide useful information that is otherwise difficult to measure.

The models used in this research were designed to represent an internal diseased carotid artery. A material such as latex, composed of bending properties similar to a carotid artery in situ was used. Latex tubes were used because excised artery tissues tend to lose their original properties and degrade quickly [4]. Figure 8 shows a picture of the rigid model (RM) and PDM, as well as the cross-sectional areas of the diseased portion. Figure 9 shows clinical images of stenosis of different geometries. Figure 9 (a) shows a cervical stenosis, which is similar to the rigid model because the diseased artery is experiencing symmetrical rigidity. Figure 9 (b) shows an example of a plaque dome stenosis, where the plaque is growing on one side of the wall. Table 1 compares

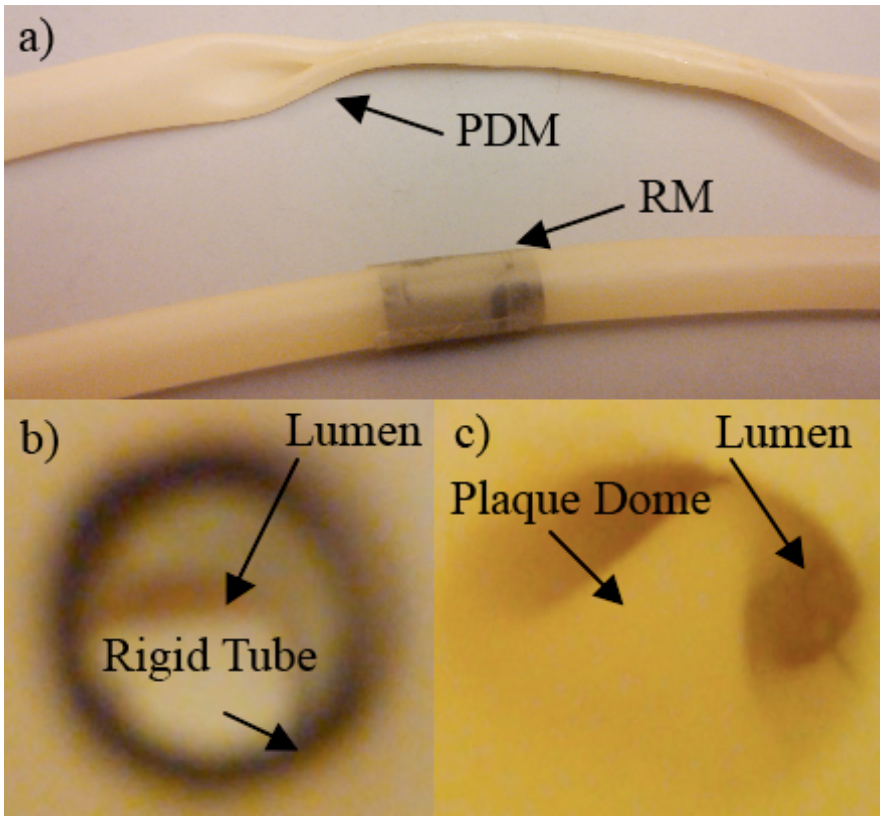

Figure 8: a) Picture of RM and PDM. b) Cross-sectional area of the RM as seen through the vessel. c) Cross-sectional area of the PDM as seen through the vessel.

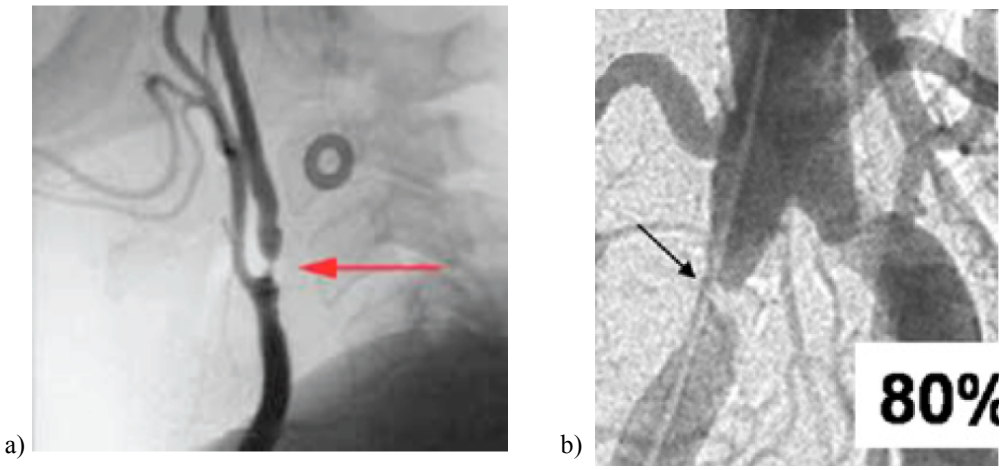

Figure 9: a) clinical image of cervical stenosis (www.ohsu.edu/dotter/carotid_stenting.htm) b) clinical image of plaque dome stenosis (Sidkar et al [34]).

Table 1: Parameters of carotid arteries of male and felmale age groups and the models. The lower and upper bounds for Young's modulus and wall thickness for each age group was used to calculate the bending modulus. Equation 3 was used to calculate the bending modulus. The models were designed to have a similar bending modulus to some carotid arteries of male and female age groups.

Age Group/Male (yr)	Lumen Diamer (mm)	Wall Thickness (mm)	Young's Modulus (kPa)	Bending Modulus (N-mm)
45-49	6.60±0.65	0.617±0.136	771±309	0.051:0.461
50-54	6.55±0.65	0.652±0.149	817±375	0.056:0.613
55-59	6.61±0.72	0.700±0.179	882±448	0.061:0.900
60-64	6.67±0.75	0.735±0.193	983±557	0.068:1.230
Models	6.35	0.381	1307	0.072
Age Group/Female (yr)	Lumen Diamer (mm)	Wall Thickness (mm)	Young's Modulus (kPa)	Bending Modulus (N-mm)
45-49	5.86±0.58	0.553±0.118	701±324	0.031:0.310
50-54	5.95±0.60	0.581±0.129	825±387	0.040:0.436
55-59	5.95±0.60	0.638±0.149	868±409	0.054:0.621
60-64	6.11±0.62	0.674±0.146	965±491	0.070:0.800
Models	6.35	0.381	1307	0.072

properties from our models to those of carotid arteries obtained through ultrasound in one study conducted on 3,321 white male and female subjects [4]. The models were designed to have a similar lumen area and bending modulus as a carotid artery. Latex has a greater Young's modulus than the carotid artery, therefore, the models were designed with a smaller wall thickness in order to have a similar bending modulus. Since an artery is curved and it has to bend when stresses are applied inside the lumen, the bending modulus is considered to study the mechanics of diseased arteries. Although the Young's modulus describes the amount of stiffness in the artery, the bending modulus is a function of curvature and describes the amount of bending. The bending modulus is the change in bending moment divided by the change in curvature, which is approximately equal to Young's modulus times the thickness cubed. The formula for bending modulus is shown in equation 3 below [26],

$$3.\ D = dM/d\kappa \sim Eh^3$$

where D is the bending modulus, M is the bending moment, κ is the curvature, E is Young's modulus, and h is the thickness of the vessel. Due to much variability in Young's modulus and wall thickness of different age groups, the model was designed to have a bending modulus of some carotid arteries, mainly those with a smaller Young's modulus and wall thickness.

2.2 Recording devices

To obtain wall motion measurements from the experimented models, a pressure sensor, a stethoscope, an optical sensor, a pulse sensor and a piezoelectric displacement transducer were used. Each device was used for different analysis depending on the

desired signal. However, they were all used to verify the mechanical behavior observed from the physical models.

The pressure sensor was used to measure the pressure across the stenosis of the artery. The pressure sensor BSL-SS19L from Biopac™ was used. The tubes connecting the pressure sensor to the pump and cuff were removed to connect the other tubing for the experiment. The pressure sensor consisted of one hose barb on each end that fit 0.25" tubes; the diameters of the vessel models were 0.25". Figure 10 shows the pressure sensor that was taken apart from the pressure cuff and bulb.

Figure 10: Biopac™ pressure sensor taken apart from pressure cuff and bulb.

An electronic stethoscope, a device from Biopac™, was used to record sounds of the vessels. This stethoscope was very sensitive and easily picked up 60Hz from the laboratory. Although adding some padding around the stethoscope can reduce the room noise, the stethoscope alone loaded the vessel enough to interfere with any sounds being produced through vibrations or turbulence.

An electrical circuit was developed to drive an optical vessel displacement sensor. This optical sensor was a reflective photosensor RPR-220 from (Rohm Semiconductor). The optical sensor consisted of an infrared (IR) LED and a phototransistor. The IR LED will send infrared light onto a reflective material placed on the surface of the vessel model, which will reflect the light to the phototransistor. Based on Ohm's law, defined in equation 4, the resistance and voltage supplied was measured to not exceed the optical sensor's current limits [31].

4. $V = I / R$

A 270Ω resistor was placed on the anode side of the LED and the cathode was connected to ground, also 9V powered the resistor. This resistor was used when 9V was supplied because the LED has a forward current I_f limit of 50mA; the LED was supplied a current of 33.3mA. The connector of the phototransistor was powered by 9V and a 470Ω resistor was connected from emitter to ground. This resistor was used since the phototransistor has a collector current I_c limit of 30mA; the phototransistor was supplied a current of 19mA. This circuit connection with the phototransistor is known as a common collector amplifier. The specs for the LED and phototransistor are shown in the table 2. Figure 11 shows the circuit for the optical sensor, and Figure 12 shows a picture of the circuit.

Table 2: Specifications for RPR-220 optical sensor

• Absolute maximum ratings (Ta = 25• C)

	Parameter	Symbol	Limits	Unit
Input(LED)	Forward current	I_F	50	mA
	Reverse voltage	V_R	5	V
	Power dissipation	P_D	80	mW
Output (photo-transistor)	Collector-emitter voltage	V_{CEO}	30	V
	Emitter-collector voltage	V_{ECO}	4.5	V
	Collector current	I_C	30	mA
	Collector power dissipation	P_C	80	mW
Operating temperature		Topr	−25～+85	℃
Storage temperature		Tstg	−30～+85	℃

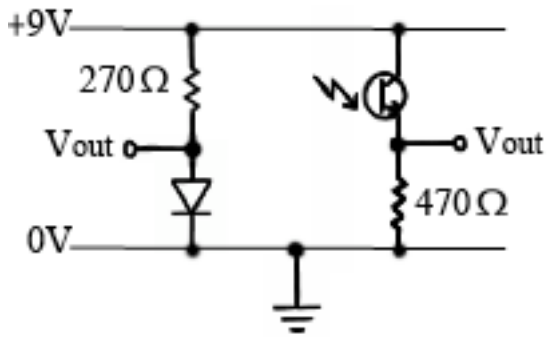

Figure 11: Circuit for optical sensor; composed of an LED and phototransistor

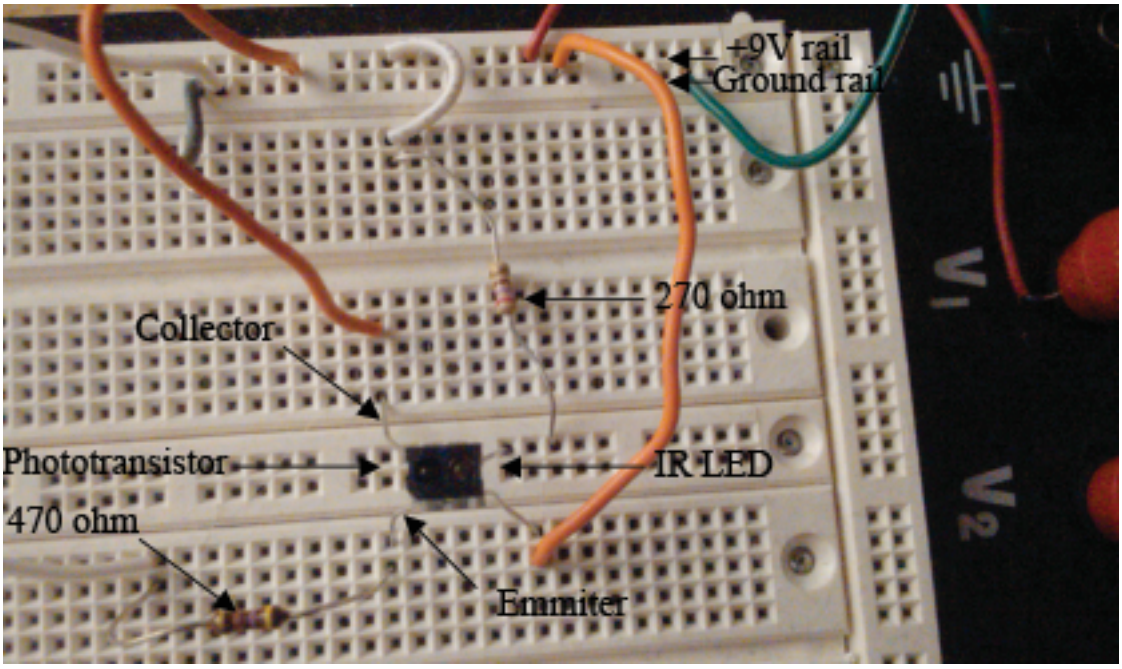

Figure 12: Picture of optical sensor circuit.

This device was able to measure large change of displacements and distance to the optical sensor based on light intensity, however, it was not able to detect relatively fast changes of displacements. Therefore, this device could not measure vibrations caused by δ small changes, but it could measure the mean deflection caused on the vessel walls of the models. This device was able to relate the amount of strain occurring on different locations of the diseased vessel models.

A pulse plethysmography from Biopac™ was also used to measure displacement, but this device did not work well for measuring higher frequencies, since it was designed to detect a blood pulse, which occurs at approximately 1 Hz. It did however, measure some frequencies in the 0-20 Hz range.

The piezoelectric material used was a polyvinylidene fluoride (PVDF) film from (AMP Flexible Filmsensors, Valley Forge, PA). The PVDF is a flexible polymer that acts like a capacitor when charge due to stress is produced on the silver ink surface of the film. Since this material converts mechanical energy to electrical energy, it was the main device used to discover dominant vibrations exhibited on the vessel wall of the flexible plaque dome model. The PVDF film is very sensitive to mechanical vibrations and it was able to pick up the pulse on a carotid artery. Figure 13 shows the pulse obtained from a carotid artery using the PVDF film. A picture of the devices used to setup the experiments is shown in figure 14.

2.3 Experimental Setup

The experiments were set up to pass a constant flow through the lumen of the vessel models and the recording devices were plugged into Biopac™ for data acquisition. The fluid used for the experiment was distilled water from the laboratory's distilled water

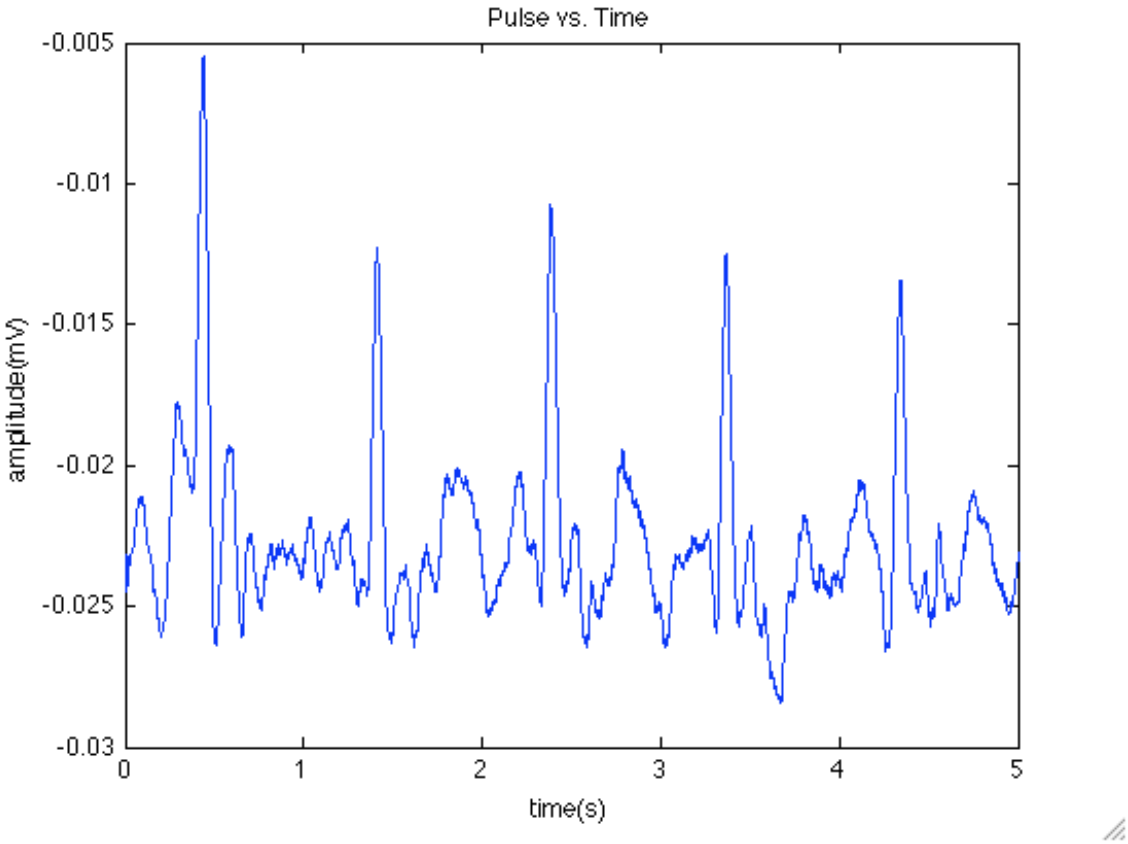

Figure 13: Pulse obtained from carotid artery using the PVDF film.

faucet. This fluid was used because it was accessible from the lab and the hose barb from the faucet allowed for a facilitated setup between the tubes that were connected. The hose barbs on each end of the pressure sensor were used to connect the tubing from the faucet and one end of the vessel models. Although water does not have the same density and viscosity as blood, the models stenosis length is used to correct for fluid properties and the mechanical behavior of diseased vessels can be observed due to the similar bending properties of a carotid artery in situ.

The flow started from the distilled water faucet to the end of the vessel model. Laboratory PVC tubing with an inner diameter of 0.5" was placed on the hose barb of the faucet. PVC braided tubing with an inner diameter of 0.25" and an outer diameter of 0.5" was used to connect the Laboratory PVC tubing and the pressure sensor. The Laboratory PVC tubing enclosed one end of the PVC braided tubing. The other end of the PVC braided tubing was attached to one end of the hose barb on the pressure sensor. One end of the vessel model, which also has an inner diameter of 0.25", enclosed the other end of

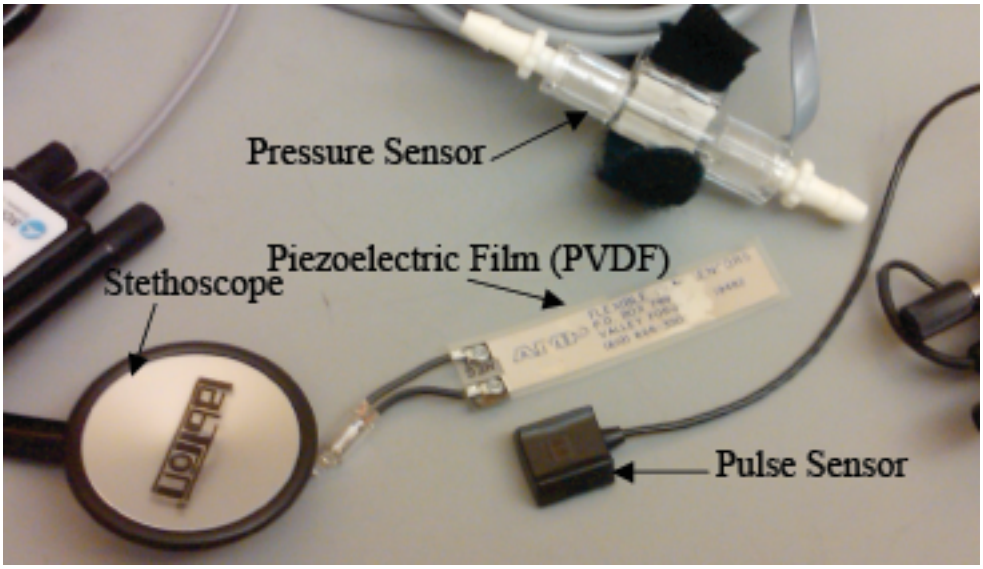

Figure 14: Devices used for recording.

the pressure sensor hose barb. The output of the pressure sensor was then connected to Biopac™ for recording. The other end of the vessel prototype was aimed towards the sink to allow water to continuously flow out. Figure 15 shows an example of the tube connections for the experimental setup.

There were various measurements applied that consisted of corresponding sensor devices. A laboratory ring stand was used to position the devices, such as the optical sensor, the pressure sensor, and the stethoscope. The optical sensor required a DC current from the power supply as input and 9V was supplied. Double-sided tape was used to place the piezoelectric film on the vessel wall of the different models. All outputs from the electrical devices were input to the Biopac™ DAQ for data acquisition.

2.4 Preliminary Experimental Protocols

This section discusses the preparatory step for conducting experiments and analyzing the results. All trials require a constant flow rate through the vessel models and the recording devices are calibrated. Once the are calibrated, different experimental protocols will be followed. These following steps are essential for obtaining accurate and meaningful results.

2.4.1 Constant Flow Rate

The distilled water in the Biomedical Engineering laboratories is delivered from a reservoir located on the roof, thereby providing a constant pressure source. The distilled water faucet valve allows for more control of the flow rate because it only depends on how much the valve opens instead of relying on pressurized water from the regular faucet. Therefore, more range of flow rates can be obtained using the distilled water faucet.

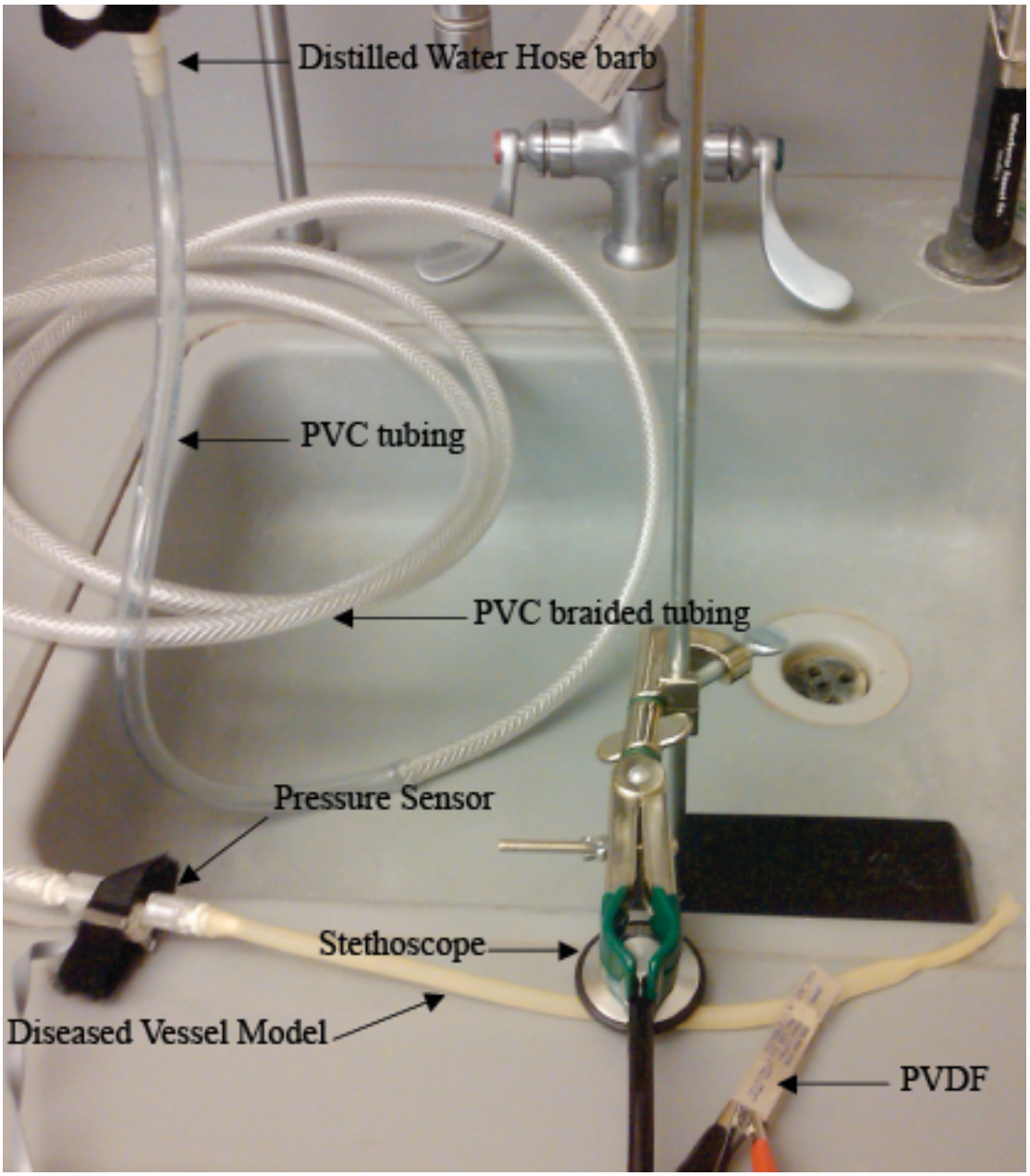

Figure 15: Example of the experimental setup.

The constant flow rate desired was 350ml/min. This is the average flow rate in the human carotid artery [11]. To obtain this flow rate, the distilled water faucet valve is opened to allow water to flow into the beaker while a stopwatch records for one minute. The valve is controlled until the desired steady flow rate is reached.

2.4.2 Calibrations

The devices used in the experiments were all calibrated differently based on the functionality of the device. Biopac™ allows the user to specify two known values for reference of calibration. Once the device is ready to measure one known value at a given specification, the user clicks on the first calibration value, the same is done for the second value.

2.4.3 Pressure Sensor Calibration

The pressure sensor was calibrated by using a pressure cuff, pump, and pressure gauge. The pressure sensor is input into Biopac™ and the appropriate channel is selected. The pressure cuff is placed around the arm and pumped to 40mmHg. This is the first calibration point input into Biopac™. Then, the pressure cuff is pumped to 100mmHg and is used as the second calibration point.

2.4.4 Optical Sensor Calibration

To test the frequency response of the optical sensor, a reflective surface was moved to and from the optical sensor at a very low frequency and at a high frequency. To test the low frequency, a reflective surface was manually moved 1 cm to and away from the optical sensor. Since this was done manually, the frequency of the movement was relatively low between approximately 0.6-1.3 Hz. A reflective material was placed on top of a radio speaker and a generator provided the speaker with a sine wave of 80 Hz.

The optical sensor could not measure rapid and small changes of displacement from the speaker. Figure 16 and 17 show the displacement versus time output from the optical sensor when it was controlled manually and the frequency response from the speaker. Figure 17 shows how the optical sensor could not pick up higher frequencies as the frequencies on the FFT attenuated at about 0.5 Hz, but was able to pick up the low frequencies from the large change in displacements.

To calibrate the optical sensor, a multimeter, power supply, and Biopac is used. A DC voltage of 9V is provided to the input of the optical sensor circuit. A probe connected to a multimeter is placed on the emitter output of the phototransistor. An output cable is connected from the emitter to Biopac. The specs for the RPR-220 optical sensor show the relative output vs. distance relationship. The output is a measure of light intensity. There is a semi-squared relationship between increasing distance and increasing light intensity, with a peak at approximately 7mm. Therefore, to get precise measurements for relative distances, the device must be placed within the slope of the relative output vs. distance relationships. This was accomplished by calibrating the device between two distances that fall within the slope range. Figure 18 shows the specs for the phototransistor.

To begin calibration, a reflective surface is placed a distance within the specs range for the sensor above the phototransistor. The height of the optical sensor is measured to calculate the approximate distance from the reflective surface. A ruler is placed on the breadboard to measure the distance from the reflective surface to the top of the optical sensor. Since the optical sensor cannot measure rapid changes of small amplitudes, the relative distance is not used as input into Biopac™. Instead the voltages

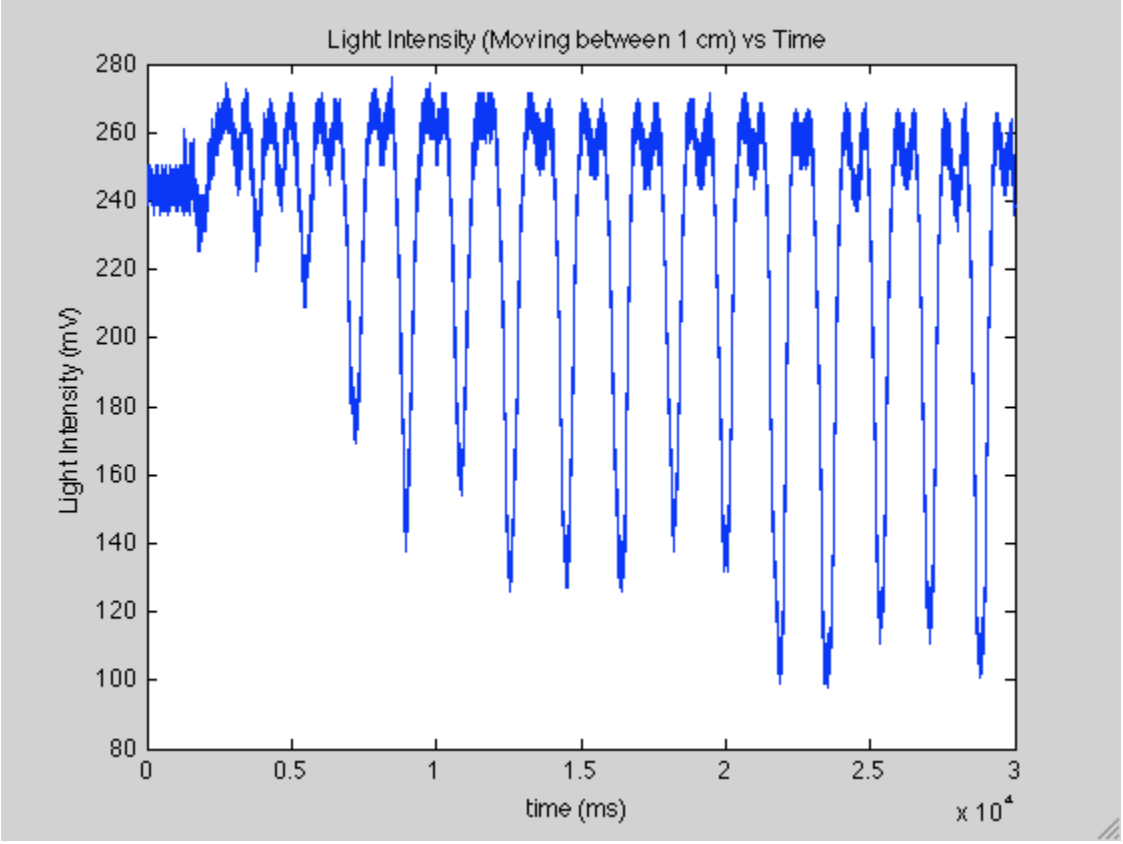

Figure 16: Light intensity verses time for manually moving a reflective surface over the optical sensor between 1 cm.

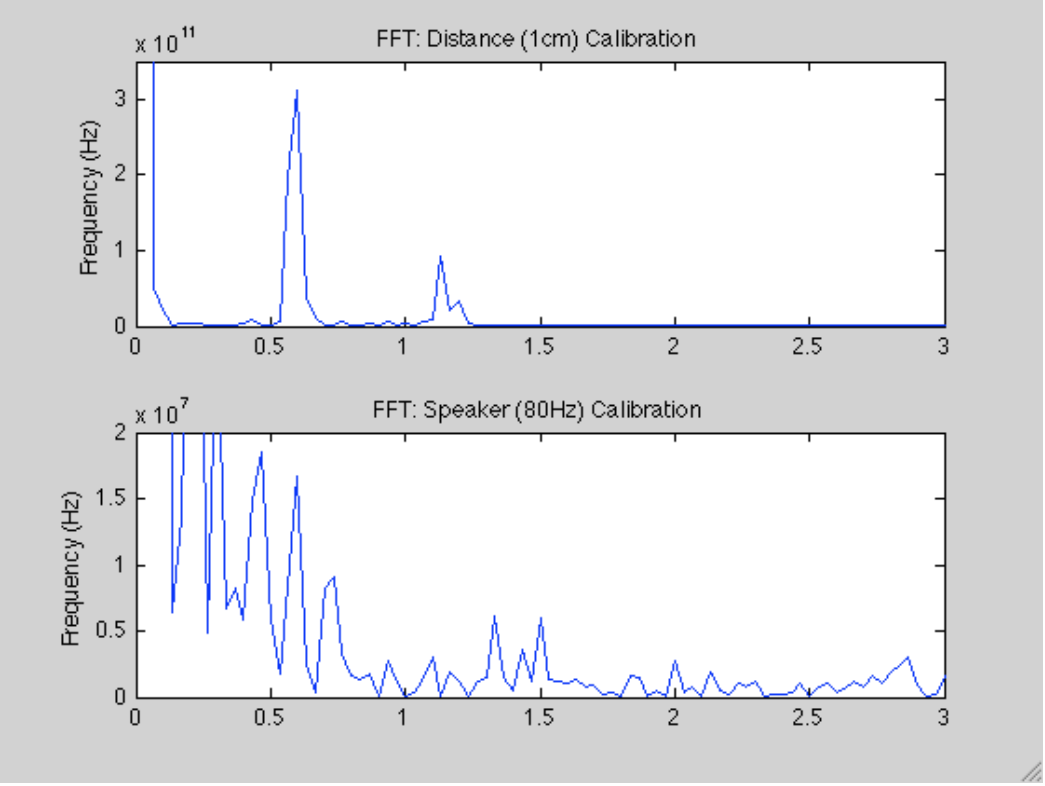

Figure 17: FFT for 2 calibration tests. (top) plot shows FFT from moving object to sensor between 1cm at~(0.6-1.3Hz). (bottom) plot shows FFT from speaker at 80Hz

read from the multimeter for the relative distances within the slope range are entered into Biopac™ so that it records the light intensity precisely. The first reference voltage entered into Biopac™ is 623mV, which corresponds to a distance δ_1 of approximately 4.14mm. The second reference voltage is 60mV, and this corresponds to a distance δ_2 of approximately 1.98mm. According to the specs shown above, a distance δ_1 should output approximately 70% of light intensity and a distance δ_2 should output approximately 25% of light intensity. This is what the optical sensor should output when the voltage supplied is 2V. However, 9V was supplied, therefore, the light intensity for

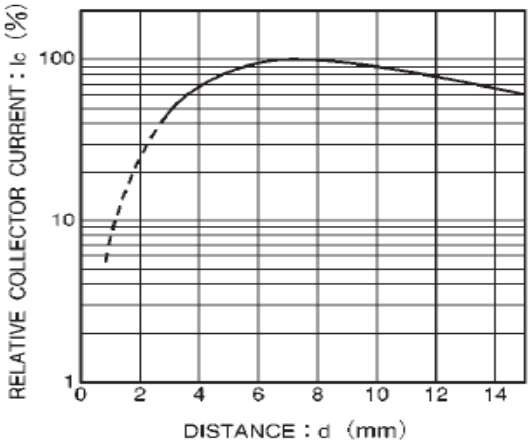

Figure 18: Specifications for optical sensor; Relating light intensity versus distance away from object.

δ_1 >> light intensity δ_2, but the output still shows an increase in light intensity per increase in distance. As seen from Figure 18, there is an inverse relationship when the distance between object and optical sensor exceeds approximately 7mm. This is sufficient to show intensity of the mean deflection in the diseased vessel models and thus show intensity of stress on the vessel walls. The optical sensor is then placed within the specs slope range above the vessel models during the experiments.

2.4.5 Plethysmography Calibration

To calibrate the Biopac™ plethysmography, a micrometer from (Central Tool Company, Cranston, Rhode Island) was used. This device was used for calibration of distance because it is a fine precision measuring tool. It was also convenient because the spindle that the pulse sensor detected has a reflective surface. The micrometer consists of a thimble in a barrel that when turned by means of a screw, moves the spindle closer or further to the anvil. The screw has 40 threads to an inch. Therefore, one complete revolution of the thimble moves the spindle up or down $1/40^{th}$ of an inch or 0.025". There are 4 spaces on the barrel, which each represent $1/10^{th}$ of an inch or 0.1". The thimble itself has 25 spaces each reading 0.025". The final reading is the sum of the highest figure shown on the barrel, number of lines visible between the number shown on the barrel and the thimble edge, and number of lines on the thimble. Figure 19 shows a picture of the micrometer.

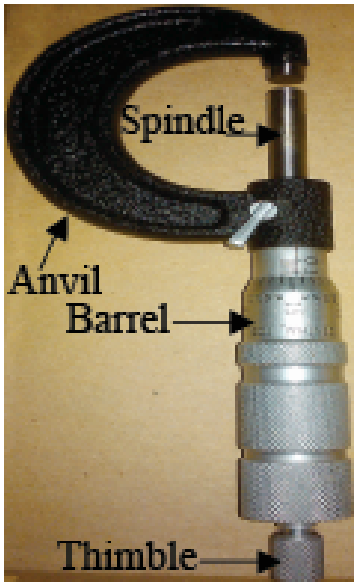

Figure 19: Micrometer used for calibrating distances from Biopac™ pulse sensor.

The pulse sensor is taped on the anvil using double-sided tape. The spindle is moved up towards the pulse sensor until it barely touches the pulse sensor. This was done initially to obtain the height of the pulse sensor, which was approximately 0.344". Then the spindle was moved 2 distances away from the pulse sensor for references of calibration into Biopac™. The first distance read 0.331", which was subtracted from 0.344", therefore, d_1 read 0.013". After subtracting the pulse sensor distance from the second distance of the spindle, d_2 was obtained, and read 0.029".

2.4.6 Stethoscope Calibration

The Biopac™ Stethoscope was calibrated using 2 tones for reference. The tones were obtained from a Motorola Blur cell phone. The "digital phone" ring tone was used because the signal is the same for duration of time. For one reference of calibration, the tone was set to twice the volume as the other tone. This will allow the stethoscope to distinguish louder sounds.

2.5 Experiments

The models are subjected to a constant flow, and the wall vibrations, pressure across the vessel, and sounds produced by the vessel are recorded and analyzed. Different experimental protocols were conducted to observe the models behaviors, and their corresponding devices were used.

2.5.1 Experiment with Plethysmography

The plethysmography was able to measure some changes in displacement in the low frequency range. This was used to measure the rate of deflection on the stenosis. In this experiment, a constant flow rate of 350 ml/min was passed through the lumen of the diseased vessel models, and the pulse sensor was placed over the stenosis using a ring

stand. The setup was similar to the one shown in figure 15, except that the ring stand was used to hold the optical sensor instead of the stethoscope. The models were placed with the stenosis region furthest away from the pressure sensor so turbulence produced from the pressure sensor would not interfere with the results. The SPDM was used in this experiment. The results and conclusions chapter will illustrate and discuss the differences in frequency spectrum of both early stage models.

2.5.2 Experiment with Optical Sensor

The optical sensor was able to measure distance from an object very well and was used to measure the magnitude of the wall deflection. However, it could not capture very small changes of displacements and therefore, could not measure the frequency response of the wall deflection. For this experiment, the optical sensor was placed upstream of the stenosis, on the throat of the stenosis, and downstream of the stenosis of the plaque dome and rigid stage models. The flow rate used in this experiment was also 350 ml/ min. Since the optical sensor is on a breadboard, two ring stands were used to support the breadboard and keep it at the same distance away from the models. The breadboard was faced upside down and the bases of the ring stands supported each end of the breadboard. This allowed for the optical sensor to be the same distance away from the model, and thus allowing differentiating the amount of deflection due to each model.

2.5.3 Experiment with Stethoscope

The stethoscope picked up a lot of noise from the room and therefore could not distinguish the frequencies between the models very well. However, the stethoscope was calibrated to differentiate sounds by magnitude. The stethoscope was placed over the vessel, either downstream or on the throat of the stenosis of both plaque dome and rigid

stage models. The flow rates was increased to observe how the sound magnitude relates to flow rates of both models.

2.5.4 Experiments with Piezoelectric Material (PVDF)

The piezoelectric material was able to detect changes in wall deflection very well. Since the PVDF picks up charge due to stress, the signal obtained is mostly due to the vibrations. However, the PVDF picks up the most dominant vibration. The PVDF was also tested with increasing flow rate to observe the magnitude in deflection with flow rate.

2.5.4.1 Experiment A

In this experiment, the stenosis region of the models was placed far away from the pressure sensor. The piezoelectric material was placed upstream of the stenosis a sufficient distance D away from the pressure sensor to avoid turbulence produced by the pressure sensor. Figure 20 shows an illustration of this setup.

2.5.4.2 Experiment B

In this experiment, the piezoelectric material and a stethoscope were used. The stenosis region was placed close to the pressure sensor. The piezoelectric material was placed upstream of the stenosis a distance d much less than D, and placed very close to the pressure sensor, while a stethoscope was placed downstream of the stenosis. Although the piezoelectric material will capture the turbulence from the pressure sensor, a relationship between turbulence and wall deflection can be obtained. Also, the magnitude of the pressure sensor reading would be more accurate of the pressure across the stenosis since it is at a closer distance. The stethoscope was used to capture the magnitudes of the sounds produced by the models and to correlate with the pressure

sensor and piezoelectric material at different flow rates. An example of this setup is illustrated in figure 20.

2.5.4.3 Experiment C

A similar setup to that of experiment A was used for experiment C. In this experiment, the stenosis is again placed far away from the pressure sensor. The LPDM and RM were used in this experiment. The piezoelectric material is then placed at different distances from the stenosis. The PVDF was placed a distance of 3.175 mm and 6.35 mm downstream from the stenosis and on the stenosis. It was also placed at distances 6.35 mm, 12.7 mm, 19 mm, and 25mm upstream from the stenosis.

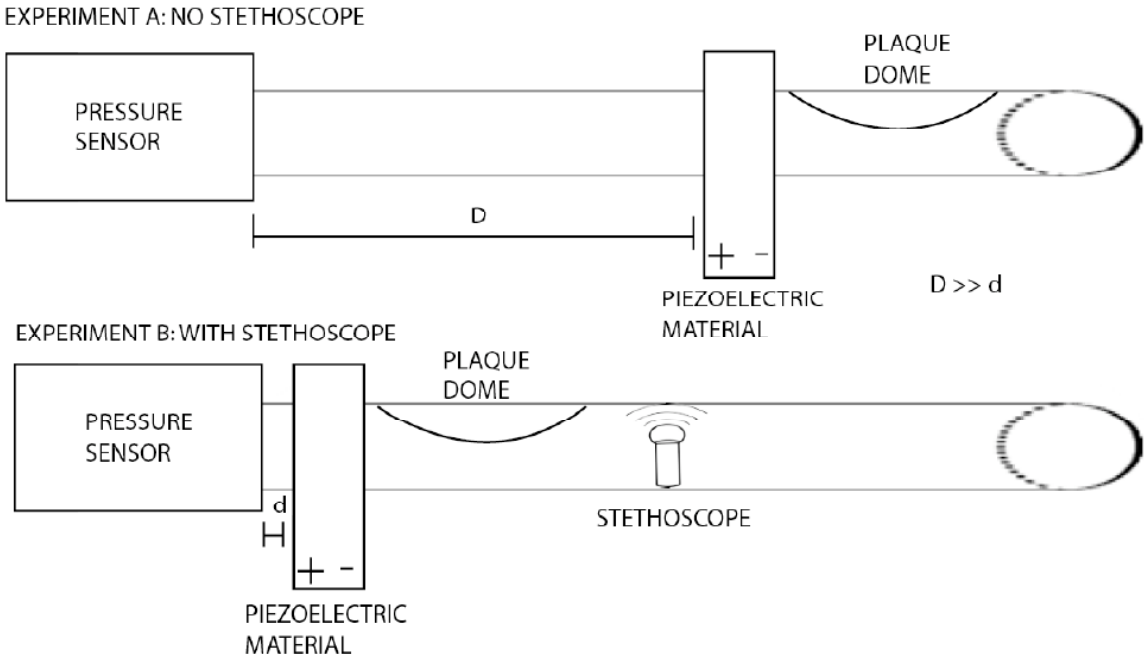

Figure 20: Experiments used with PVDF. Experiment A: Stenosis and PVDF were placed far away from the pressure sensor and upstream from stenosis. Experiment B: Stenosis and PVDF were placed close to pressure sensor and upstream from stenosis, and a stethoscope was placed downstream from the stenosis.

Chapter 3

Results

The wall mechanics and sounds produced by the RM, SPDM, and LPDM were analyzed and presented in this chapter. The longer stenosis (LPDM) showed vibrations of greater magnitude and in higher frequency ranges. This reassured that the geometry of the vessel produces wall vibrations and a greater length of the stenosis increases the vibrations. Figure 21 illustrates the difference in stenosis length for the SPDM and LPDM.

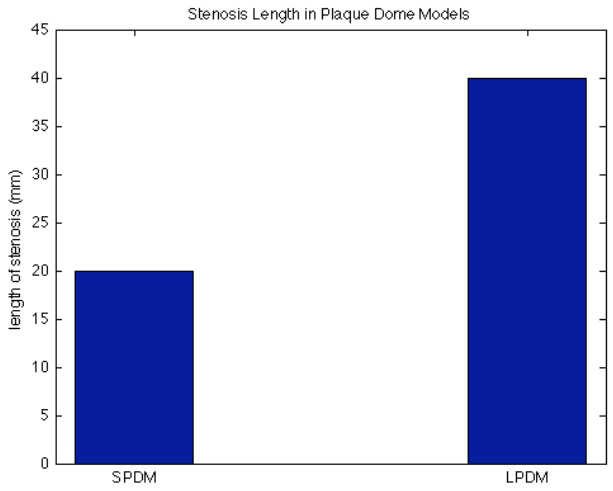

Figure 21: Stenosis length in plaque dome models: SPDM (short plaque dome model) and LPDM (long plaque dome model)

3.1 Plethysmography results: Frequency-time spectrum of wall mechanics upstream

The wall deflection of the SPDM was obtained using the Biopac™ plethysmography. When comparing the SPDM with the LPDM, the shorter stenosis length showed vibrations in the lower frequency range. The plethysmography was used to compare the wall deflection upstream of the RM and the SPDM. Figure 22 shows the FFT power spectrums for both models. The results show that RM showed a broad range

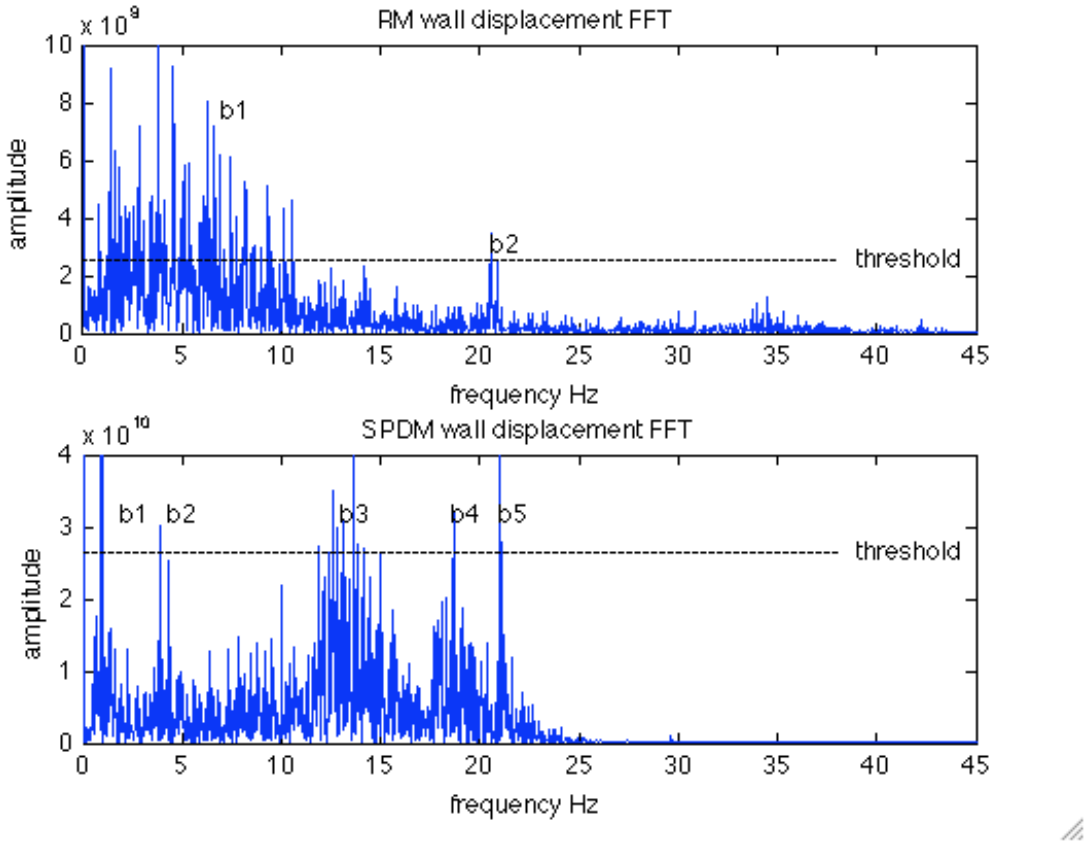

Figure 22: Power spectrum of plethysmography. (Top) FFT power spectrum for RM. (Bottom) FFT power spectrum for original SPDM.

of vibrations in the low frequency range, between 0-10 Hz. The SPDM showed a broader spectrum of vibrations occurring in frequencies between 0-22 Hz. There are approximately 4-5 frequency bands in the SPDM. These frequency bands b1, b2, b3, b4, and b5 are the predominant frequencies shown in figure 22 and all fall below the hearing range for healthy young humans; 20-20000 Hz [32]. The RM only has 2 primary frequency bands b1 and b2, and the frequencies in b1 are more concentrated when compared to other frequency bands in the SPDM.

The frequency results from figure 22 can be viewed with respect to time. A continuous wavelet transform (CWT) converts a signal from a time domain into a frequency-time domain. A wavelet with a characteristic frequency is convolved with the signal. The output of the convolution will show how correlated the frequency from the wavelet is to the signal. If that frequency is present and has a high amplitude, the output will show a high wavelet coefficient and vise versa. The wavelet can be scaled to have different frequencies, therefore, the higher scales correspond to lower frequencies and the lower scales correspond to higher frequencies. Observing the frequencies of wall vibrations in the time domain will help describe the dynamics of the system.

Figure 23 and figure 24 show the CWTs in the 2-6 Hz and 10-25 Hz range for the RM and the SPDM using the plethysmography. The “jet” colormap in Matlab® was used in the figures, and red corresponds to high wavelet coefficients and blue corresponds to low wavelet coefficients. It can be seen from figures 23 and 24, that high wavelet coefficients occur more frequent in time for the SPDM. The results show that the RM produces vibrations for a short period of time and after a longer period of time the vibrations return. For the RM, the CWTs show that frequencies occur predominantly in

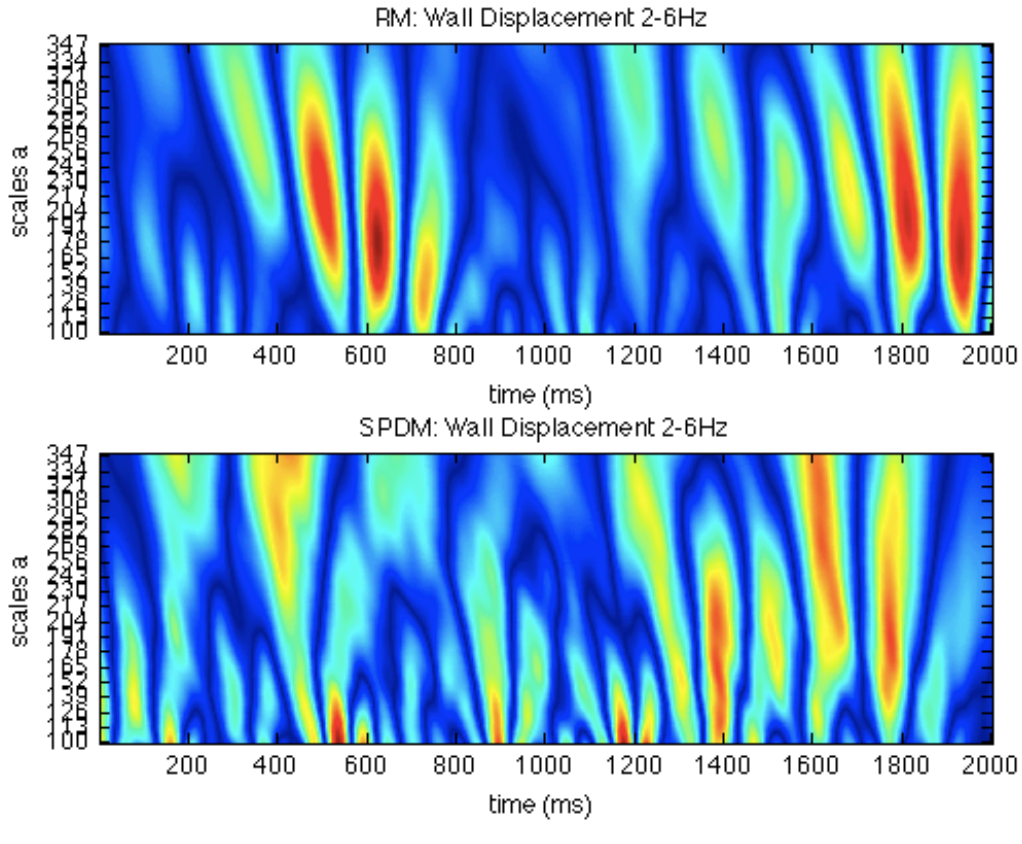

Figure 23: CWT of wall displacement using the plethysmography: scales equivalent to 2-6 Hz. (Top) RM (Bottom) SPDM.

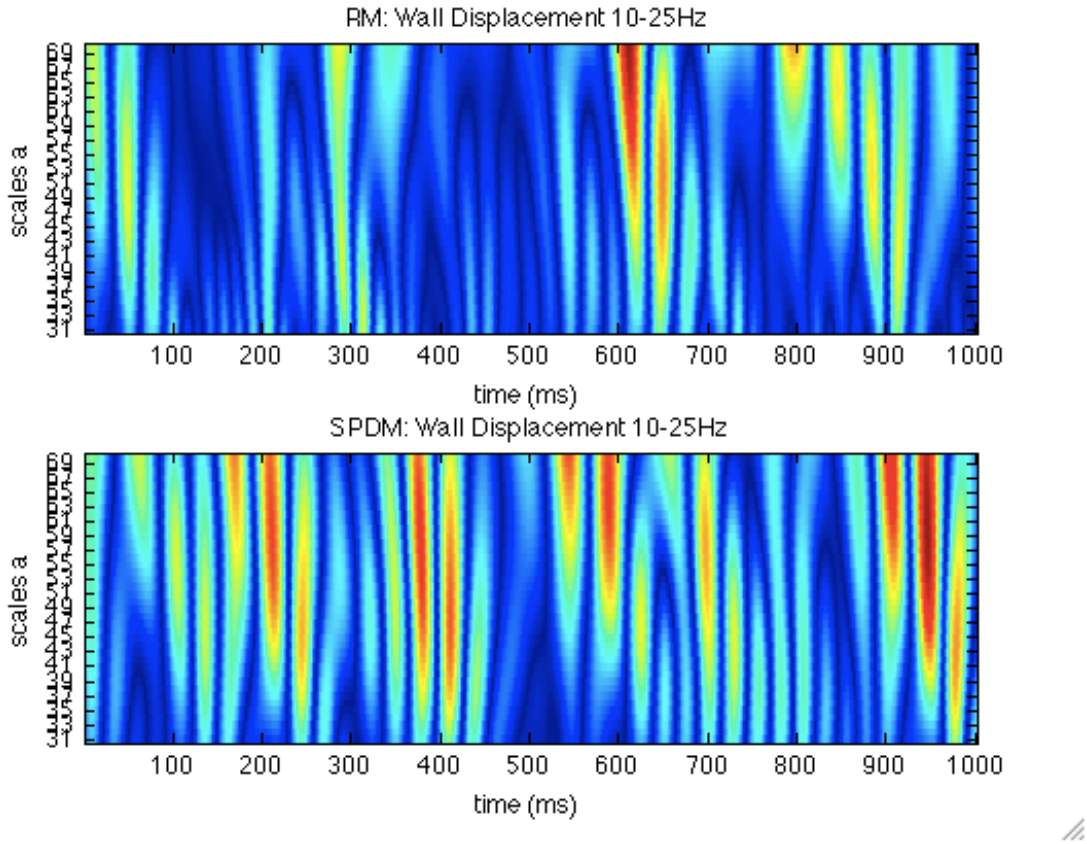

Figure 24: CWT for wall displacement using plethysmography: scales equivalent to 10-25 Hz. (Top) RM (Bottom) SPDM.

the 2-6 Hz frequency range. The SPDM has frequencies occurring for a longer duration of time. Also, in the SPDM frequency bands vary in the 2-6 Hz range, whereas frequency bands are more steady in the 10-25 Hz range. The RM also shows some similar frequencies occurring in time in the 10-25 Hz range, but the frequencies are less amplified and occur after longer periods of time.

3.2 Optical sensor results: Wall deflection upstream, on stenosis, and downstream

The optical sensor is a very sensitive device in measuring distance away from an object by the amount of light intensity. The optical sensor was placed approximately 10 mm from the models; the data shown in chapter 2 in Figure 18 indicate that a greater light intensity indicates that the object is closer to the optical sensor and therefore has a greater deflection. Figure 25 shows the light intensities obtained by the optical sensor at locations upstream, downstream, and centered on the stenosis. The upstream and downstream locations were approximately 6.5 mm from the stenosis. For both models, there was less wall deflection on the throat of the stenosis. The light intensities from upstream to stenosis dropped proportionally in both models, which may be due to the identical bending properties. The results clearly show that the LPDM has greater wall deflection in all locations when compared to the RM. The walls of the LPDM deflected more than twice as much. It can be seen from figure 25 that symmetrical rigidity of the vessel resists wall movement. The results also show that the wall deflection upstream and downstream from the RM is approximately the same. This probably occurs since the stenosis in the RM is completely symmetrical. The LPDM does not show similar light intensities upstream and downstream since the geometry of the stenosis is not symmetrical. The LPDM also showed greater wall deflection

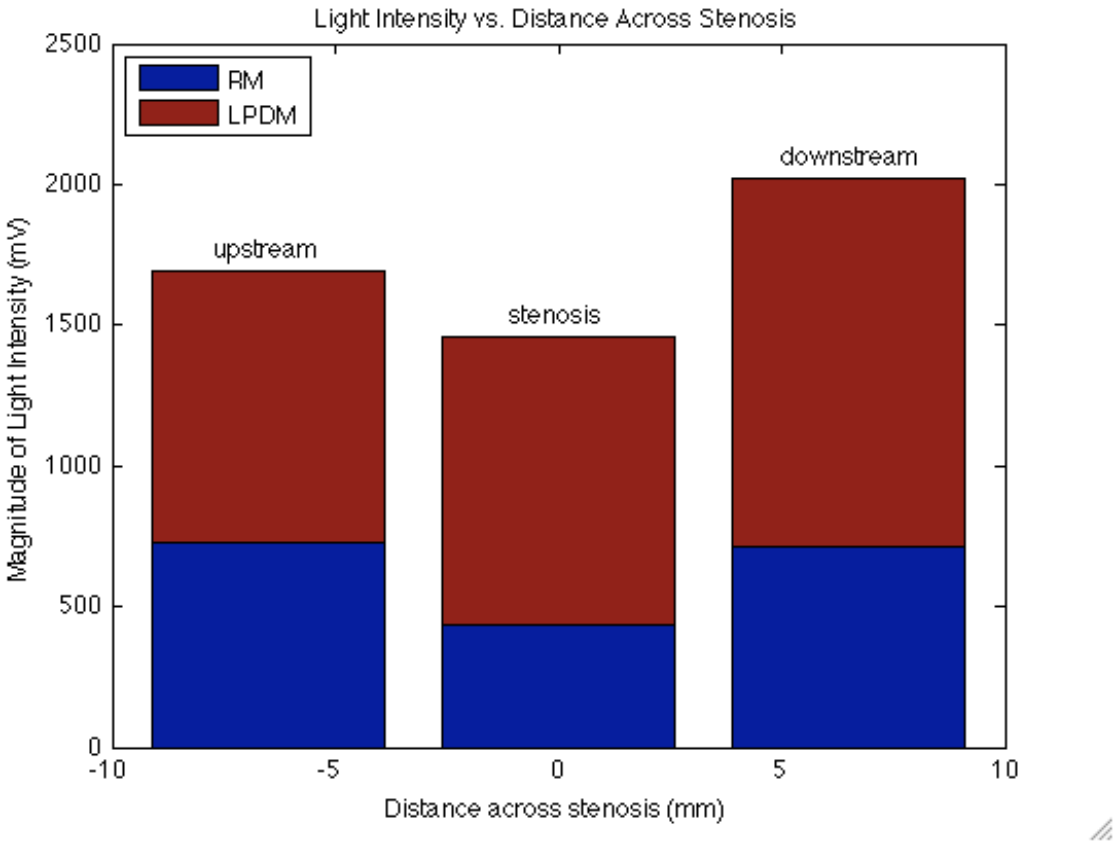

Figure 25: Magnitudes of Light intensity for data recorded upstream (-6.5 mm), on throat (0 mm), and downstream (6.5 mm) of stenosis for both models. Higher light intensities correspond to greater wall displacements.

downstream. This is possibly due to both the anti-symmetry of the stenosis as well as the turbulence that is produced at the exit of the stenosis.

3.3 Stethoscope results: Relationship with sound magnitudes

The Biopac™ stethoscope has a resonant frequency at 60 Hz and harmonics of 60 Hz. The frequency spectrums for both models were nearly identical since the stethoscope resonates at the same frequencies. The CWTs of the stethoscope recordings showed a similar frequency-time relationship to that of the wall movement. It can be seen from figure 26 that the sound frequencies produced in the RM decay with time and the period between sounds is greater than the LPDM. The CWTs for the LPDM show that there are shorter periods between sounds, and frequencies occur longer and unsteady throughout time. Another observation made is that the RM had a broader band of frequencies and higher frequencies; 36-104Hz. The early stage had a less broad band of frequencies in the 15-66 Hz range.

3.4 PVDF results: Relating deflection, vibration, and frequencies in time

The PVDF results showed differences between the amount of bending between both models. As the flow rate increases, the volume increases, and therefore, the amount of deflection occurring in the walls is proportional to the total increase in volume. The PVDF was placed upstream from the stenosis to observe wall deflection while the flow rate is increased. Figure 27 shows the magnitude of the PVDF for increasing flow ratesfor both models. It can be seen from figure 27 that the walls of the LPDM deflected more with increasing flow rates. Similar to the observations made from the results obtained from the optical sensor, the PDVF also shows how symmetrical rigidity prevents the walls from bending, thus reducing the amount of vibrations. Also, since the

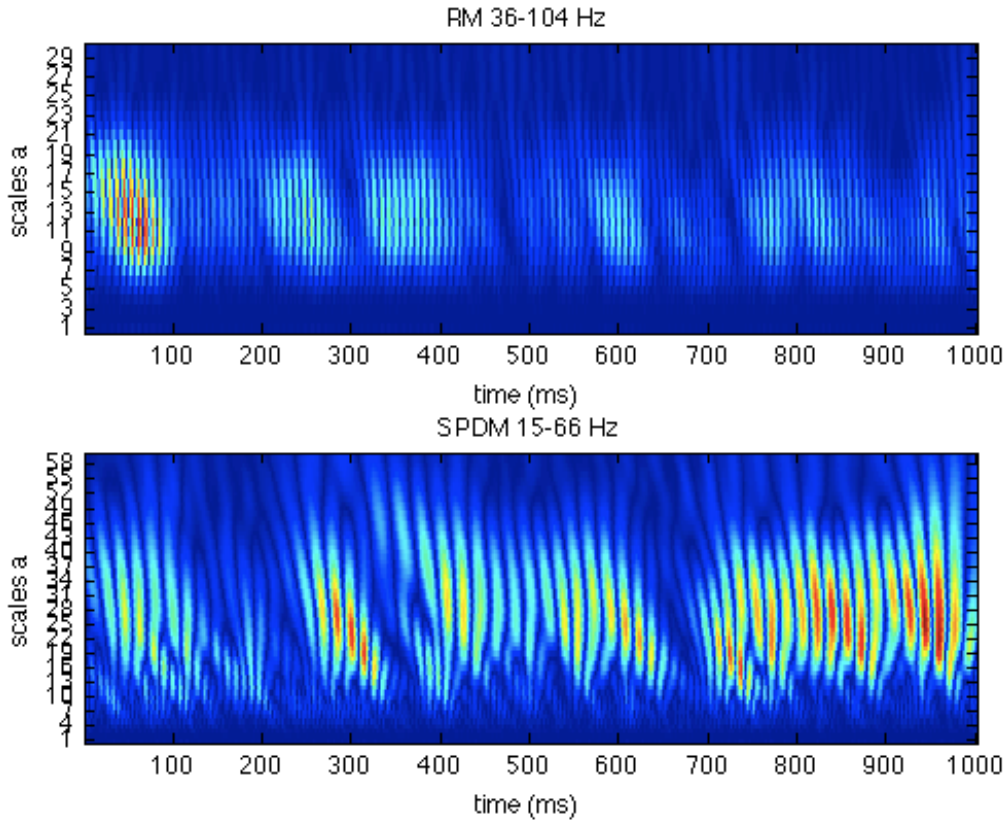

Figure 26: CWTs of stethoscope recordings. (Top) RM. (Bottom) SPDM.

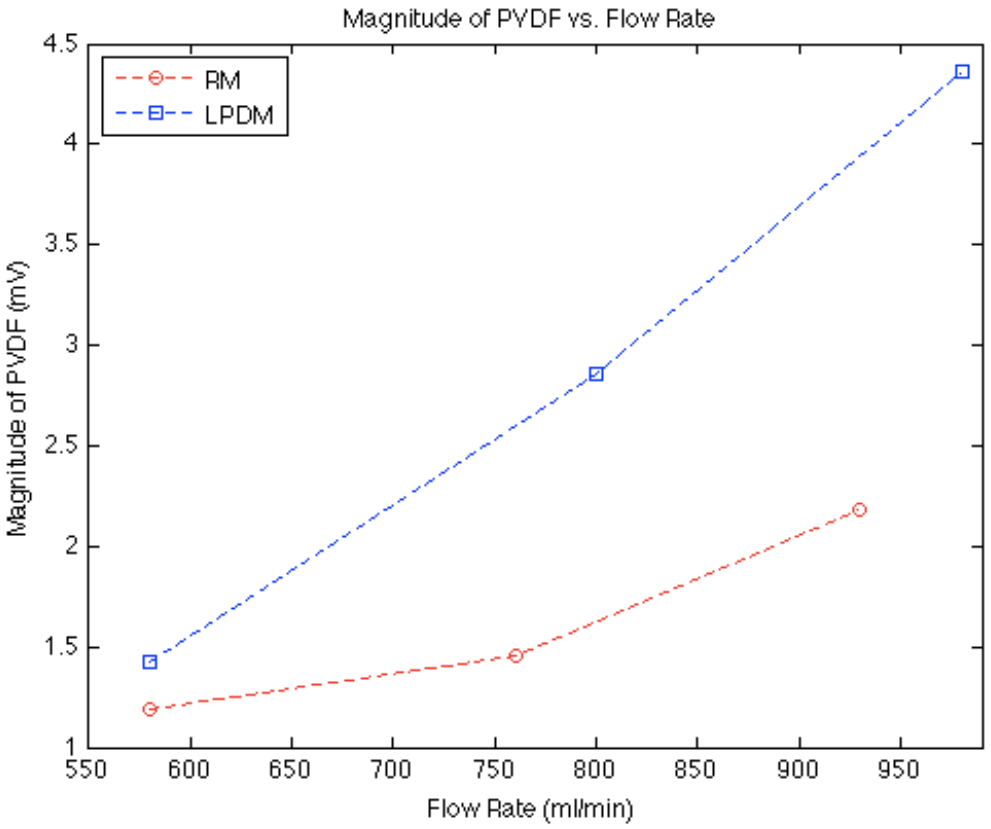

Figure 27: Magnitude of PVDF versus flow rate. (Blue) LPDM (Red) RM

walls deflected more for the LPDM, there is more volume per flow upstream from the stenosis.

Relationships between the amount of wall deflection verses distance can be made with the use of the PVDF. Figure 28 illustrates an experimental setup for measuring wall deflection along several distances from the stenosis. In experimental setup A, in Figure 28, the measurements from stenosis are with respect to the rigid portion of the disease section, and experimental setup B is with respect to the flexible portion, which is only applicable for the PDMs. Figure 29 shows that the least wall deflection occurs on the rigid center of the stenosis and the greatest wall deflections occur upstream and downstream from the stenosis. Also, as the distance from the stenosis increases, the wall deflection decreases. Another relationship that can be made from distances away from the stenosis is the frequency characteristics. The frequencies from the PVDF show a change with distance from the stenosis. It can be seen from the FFTs shown in figure 30 that lower frequencies occurring in the 10-40 Hz range become prominent with further distance upstream from the stenosis. This is also true in the RM model. When the flow rate was increased to 1100ml/min, the RM exhibited wall vibrations. Figure 31 shows how the frequencies become lower as distance upstream increases. The frequencies in the RM are more concentrated and shift slightly when compared to the LPDM.

3.5 Affects due to length of stenosis

The affects of a longer stenosis was observed. The results show that there is a frequency-shift relationship with length of stenosis. It can be seen from figure 32 that the vibrations are now audible, occurring at approximately 45 Hz. These vibrations were

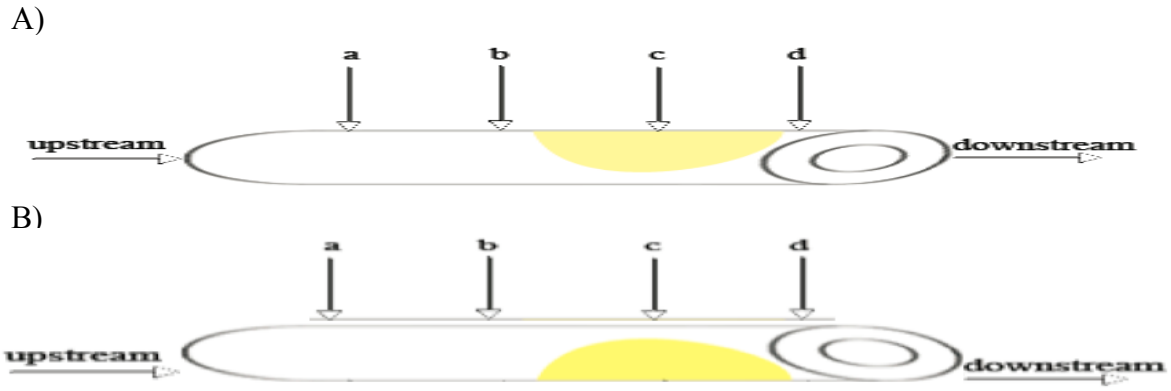

Figure 28: Location of measurements with PVDF. A) With respect to rigid portion (c) of disease section B) With respect to flexible wall (c) of disease section

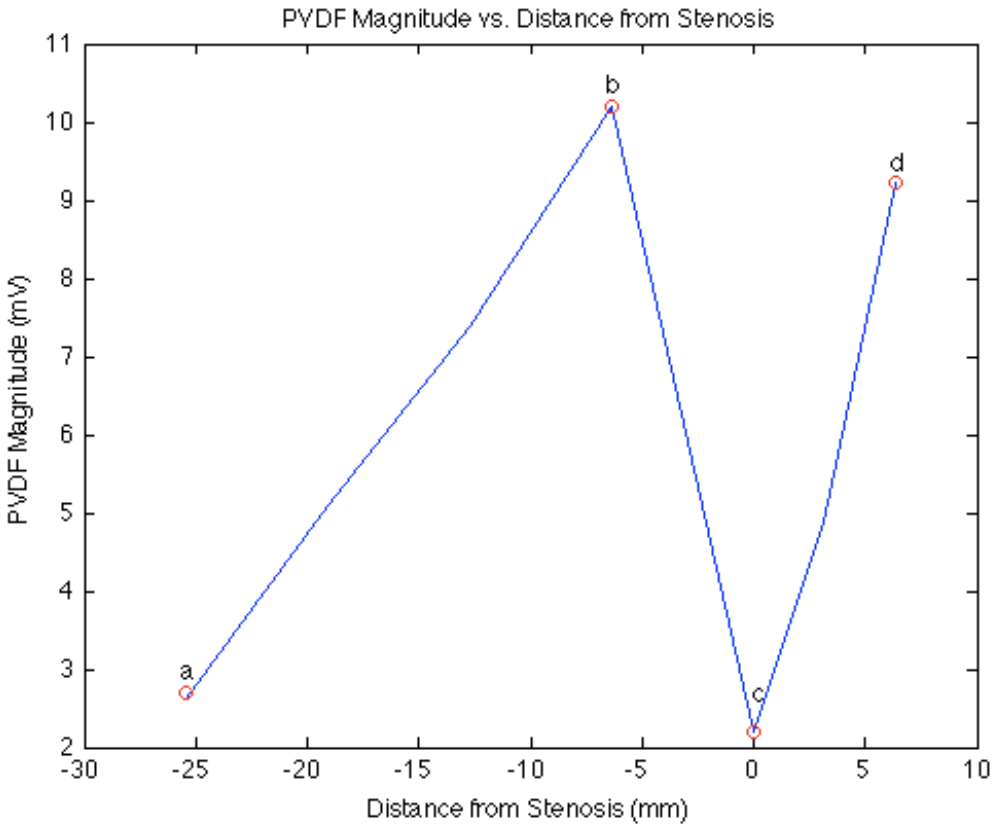

Figure 29: Magnitude of PVDF from locations indicated in figure 28A for LPDM.

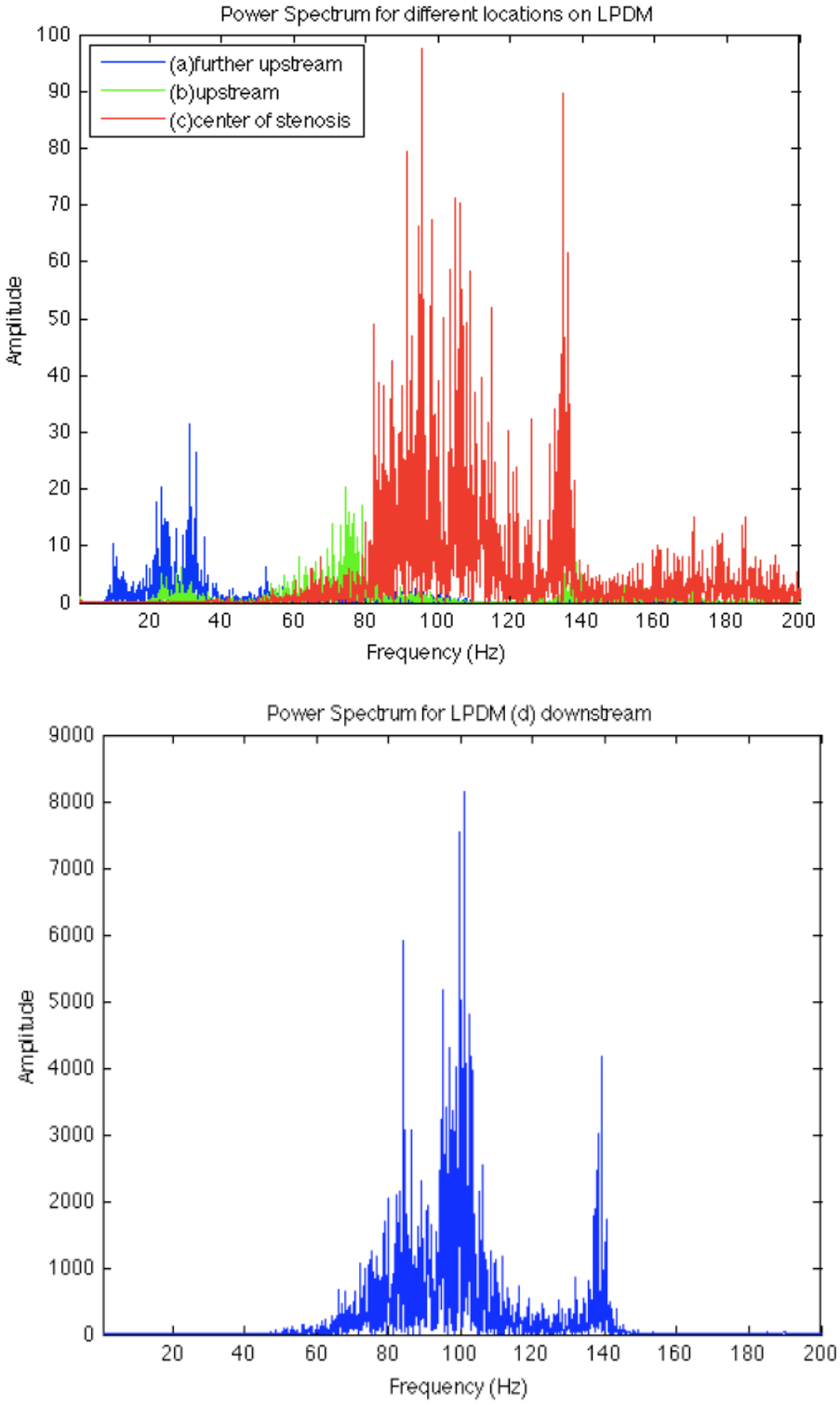

Figure 30: FFTs of PVDF for locations indicated in figure 28B in the LPDM at 1030 ml/min (top) locations a, b, and c (bottom) lodation d, downstream; much greater scale

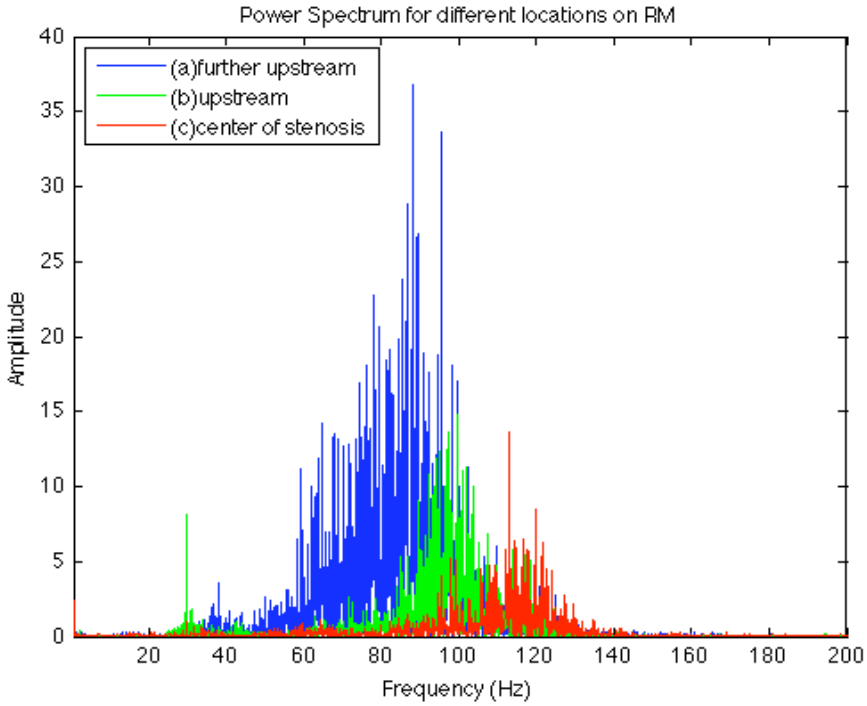

Figure 31: FFTs of PVDF for locations indicated in figure 3.7A for the RM at 1100ml/min

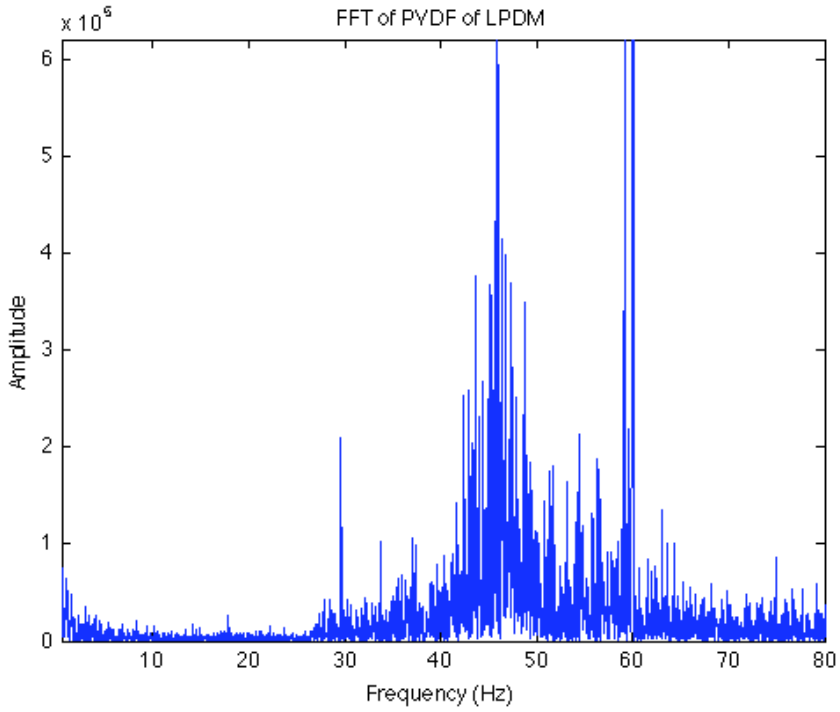

Figure 32: FFT of PVDF of LPDM, measuring wall vibrations at 350 ml/min

observed when the stenosis was far away from the pressure sensor. Two experiments were conducted using the longer stenosis, experiment A and experiment B. In experiment A, the stenosis was placed far away from the stenosis so that turbulence from the pressure sensor would not interfere. However, the stenosis was placed close to the pressure sensor to observe vibrations produced by the turbulence of the pressure sensor. It can be seen from figure 33 that the pressure and PVDF FFTs do not fall in the same range. However, when compared to the RM, the correlations between the pressure sensor and PVDF show there is more correlation in some time lags as shown in figure 34.

To observe the turbulence produced by the pressure sensor, the FFTs for the pressure sensor only were observed at increasing flow rates. Figure 35 show that turbulence from pressure sensor occurs in the 80 Hz range which become prominent at higher flow rates. Figure 36 shows the frequency response of the PVDF for the early stage model for experiment B. When the stenosis is placed close to the pressure sensor, the model vibrated more in the 80 Hz range; frequency responses for both devices were observed in figure 37. The PVDF and pressure sensor recordings were filtered at 60-90 Hz and then plotted against each other. Figure 38 show a squared relationship between the turbulence produced by the pressure sensor and wall vibrations.

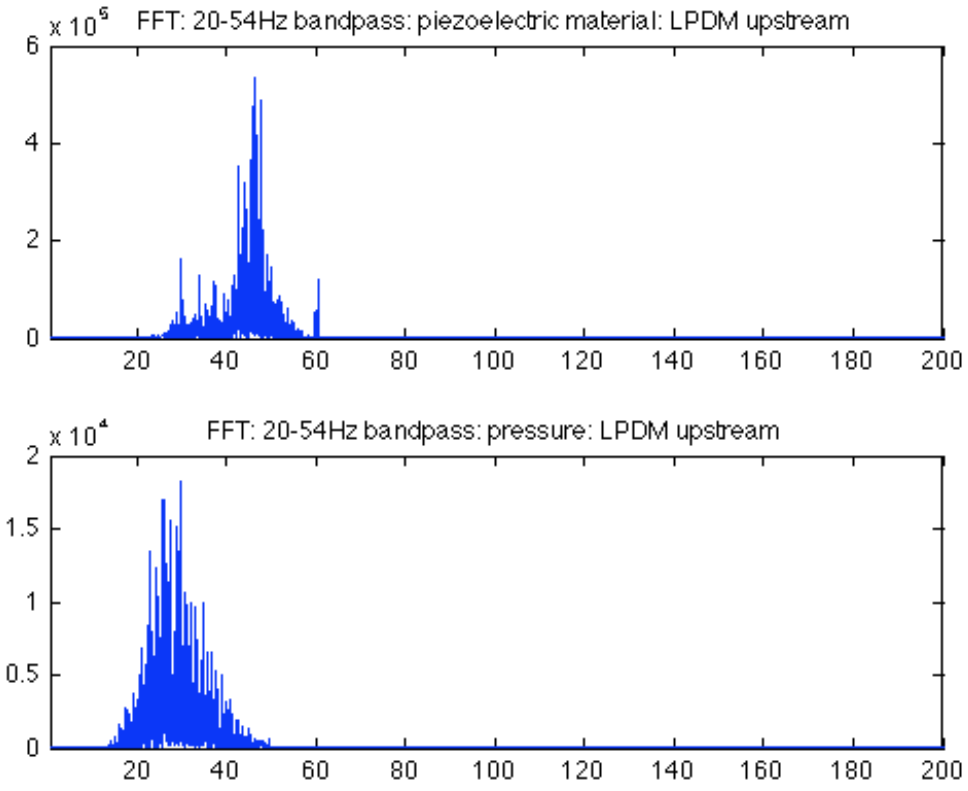

Figure 33: Frequency relationship between PVDF and pressure sensor for experiment A. (Top) FFT of 20-54 Hz band-pass filtered PVDF for LPDM. (Bottom) FFT of 20-54 Hz band-pass filtered pressure signal.

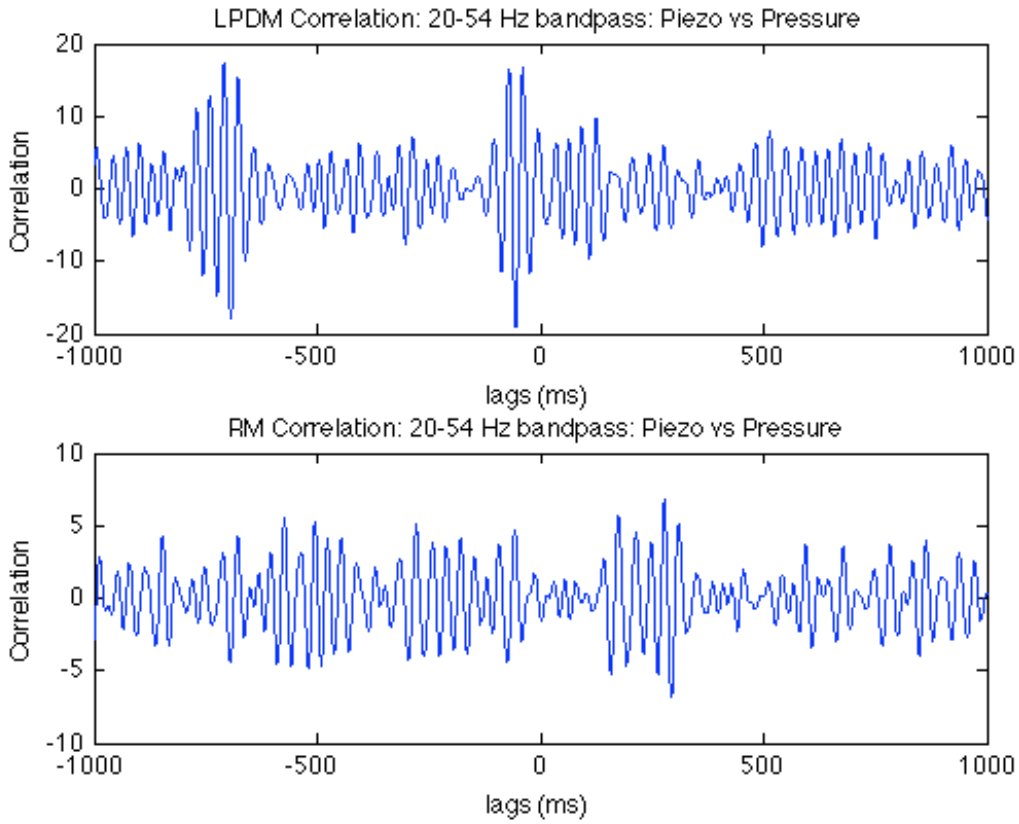

Figure 34: Correlation between 20-54 Hz band-pass filtered PVDF and pressure sensor. (Top) LPDM (Bottom) RM

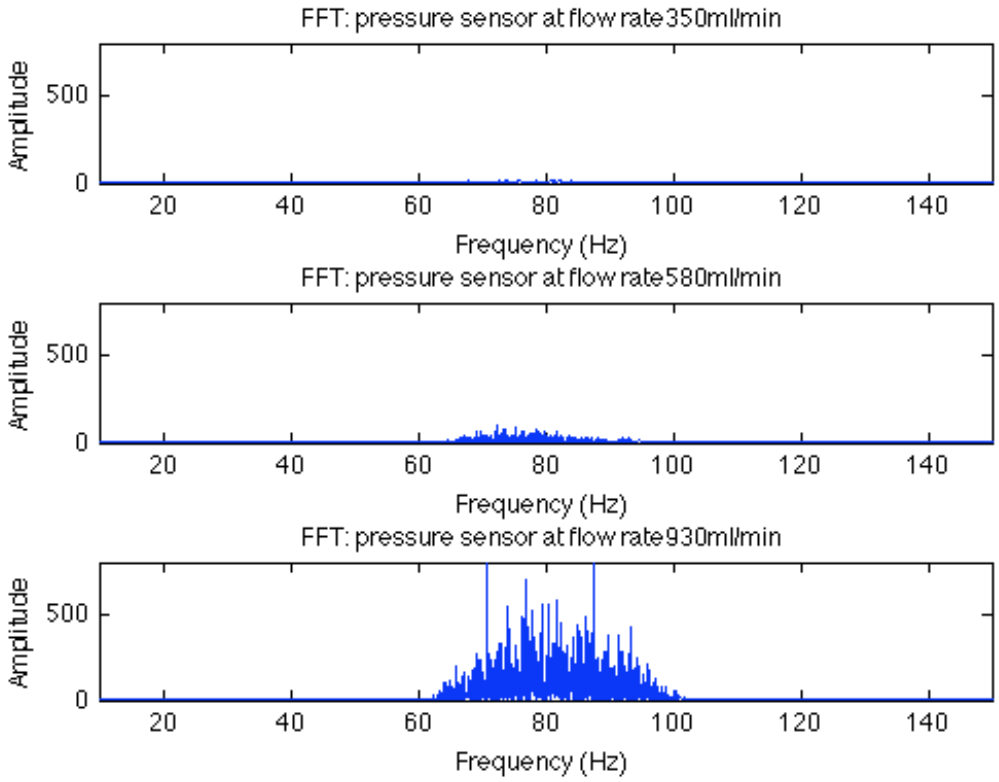

Figure 35: FFTs of pressure sensor only with increasing flow rates.

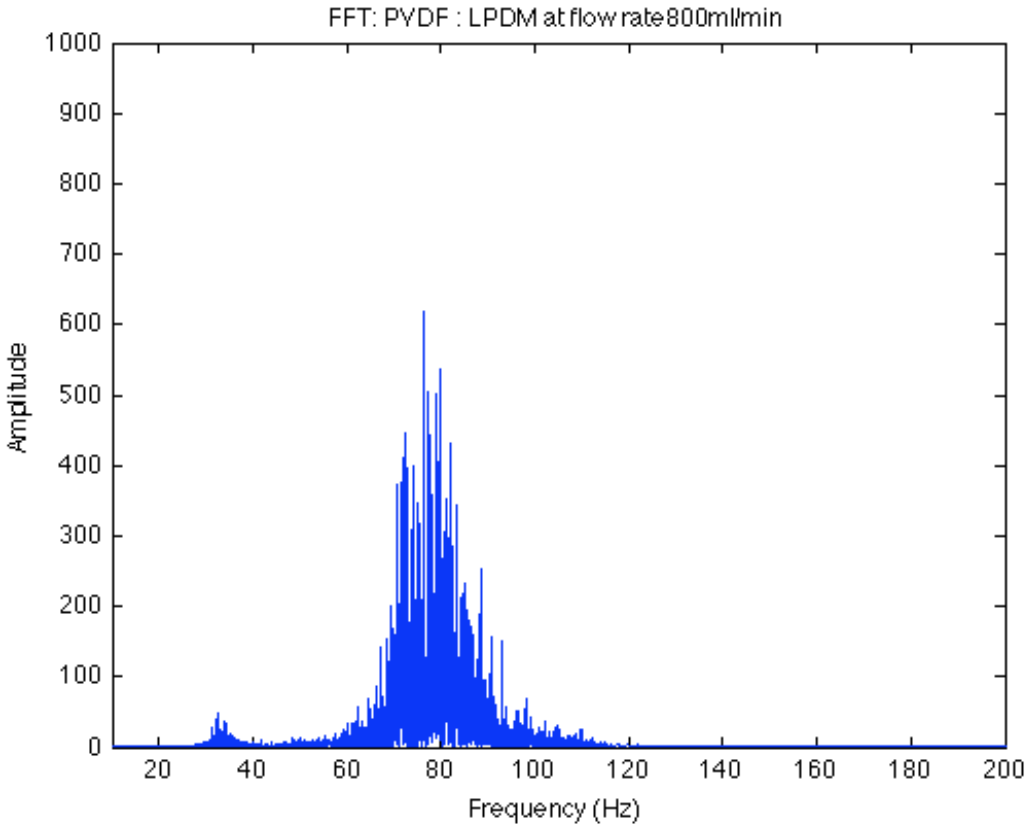

Figure 36: FFT of PVDF from LPDM with experiment B setup.

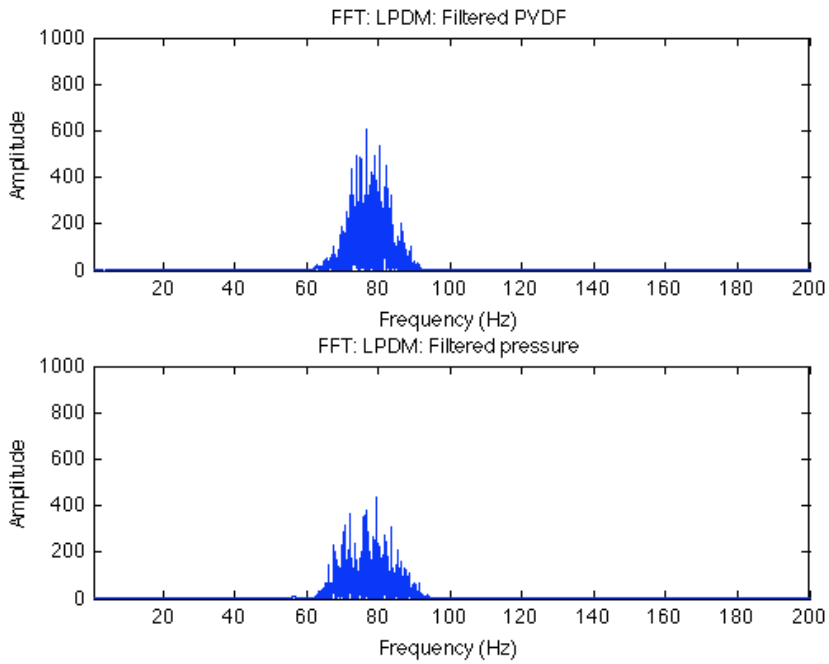

Figure 37: Frequency relationship between PVDF and pressure sensor for experiment B. (Top) FFT of PVDF for LPDM (Bottom) FFT of pressure sensor.

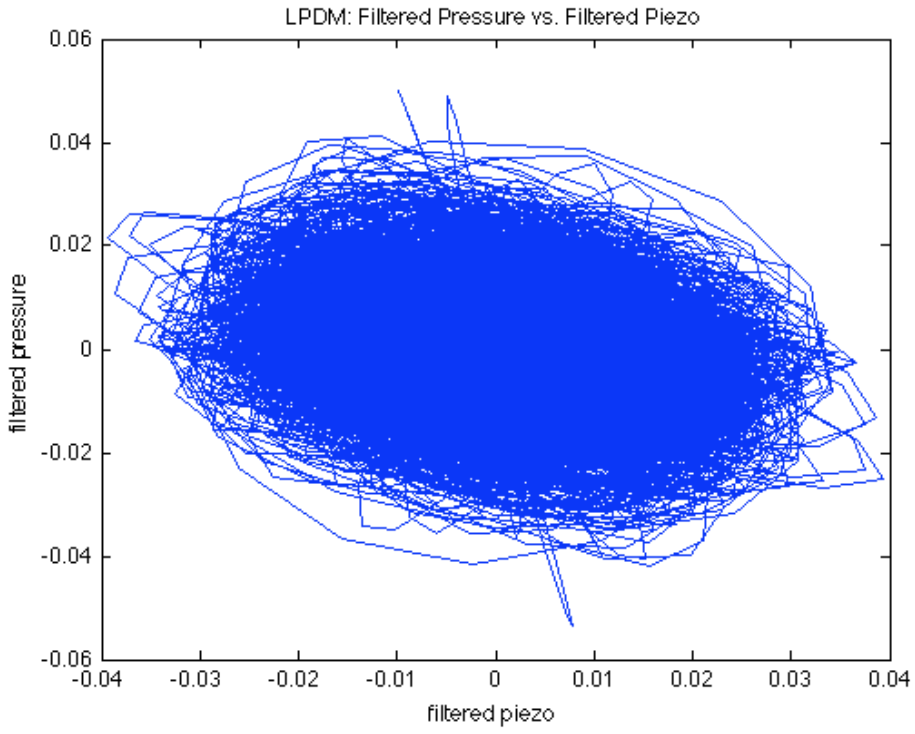

Figure 38: Filtered pressure signal versus filtered PVDF.

Chapter 4

Discussion

Vascular stenosis models can be used to explain the hemodynamics, mechanics, and other phenomena related to the disease. Several models of obstructed vessels have been developed to describe the abnormal behavior of diseased arteries, but the exact mechanism of the disease is not well understood. In this chapter, the results from the models designed for this research are discussed and compared to prior mathematical, computational, and physical models of stenotic arteries. All models have some advantages and limitations, but physical models allow for accurate measurements of velocity profiles and vessel mechanics via sensor devices.

Most computational models are based on mathematical equations without fluid dynamic assumptions. The fluid dynamics of diseased vessels are known to be very difficult to solve in closed form. There are various mathematical models for flow and wall deflection, thus, combining the equations may produce different results. An example of this is two studies that use similar equations for flow, but consider blood as different fluids and use different equations for wall properties. In a study done by Tang et al [29], cyclic artery compression was studied using a 3 dimensional unsteady model with fluid structure interactions. The mathematical equation used here to describe flow is the Navier-Stokes equation, with the assumption that the fluid is incompressible, laminar, Newtonian, and viscous. They use the tube law and a thin shell model to determine wall motion. Their results showed that the highest shear stresses occurred at the throat of the stenosis. Another study that agrees with these results is that from Ai et al, who found

higher wall shear stresses at the throat of the stenosis using an ultrasound transducer [19]. The fluid assumptions are contradicting for Tang el al [29], since viscous fluids are considered non-Newtonian, and in blood, viscosity changes with velocity, therefore, blood is considered a non-Newtonian fluid [33]. The findings from Tang et al and Ai et al are contrary to what other studies showed; there are higher wall shear stresses right around the stenosis, upstream and downstream, but lower on the throat [3], [20], [24]. A study conducted by Sen et al, also used the Navier-Stokes equation to solve for flow, but considered the fluid as incompressible and non-Newtonian [3]. Sen et al applied the classic Kelvin-Voight model for an artery with a relatively thin wall. The results showed them the opposite as Tang et al and Ai et al. For Sen et al, the locations with the lowest shear stress occurred at the throat of the stenosis. Some research concerning wall shear stresses have shown to contradict each other based on mathematical models or even the properties of the physical models used. Hence, the prior computational fluid models may not be reliable.

In this research, the physical models were designed not only to simulate circulatory flow in situ through a tube, but to study the change in the amount of structure dynamic response. This eliminates a major assumption of the computational fluid dynamics (CFD) models that is constant do to no wall motion boundary conditions. The diseased vessel models were designed to have a similar bending modulus to that of a carotid artery in situ, therefore, these models are the first dynamic models. These models can show the amount of radial stress occurring around the stenosis, as opposed to shear stress, and can be physically measured with sensor devices to confirm the amount of bending.

The variations in the computational models discussed above show that mathematical equations rely heavily on rigid boundary conditions. The contradictions in wall shear stresses between the studies mentioned above may be due to inaccurate geometry descriptions. These variations in design can be due to disease geometry or mechanical properties. For instance, Tang et al obtained the elastic properties of an arterial wall from a polyvinyl alcohol hydrogel stenosis model to create the 3 dimensional model. According to Tang et al, they used polyvinyl alcohol hydrogel because it has the same mechanical properties as a bovine carotid artery. This will create inaccuracies in the computations because not only is it not a human carotid artery, the excised tissue will lose all its original properties [4]. The results from Ai et al also agreed with the study from Tang et al. In the model, Ai et al used a plaque dome model made of araldite 5 minute epoxy adhesive, dextran mixed in saline to have a solution as the same density as blood, but did not mention what tube they used. Ai et al state that as a corollary, from high velocities measured at the throat, there are highest shear stresses at the throat.

The mechanics of diseased arteries have been studied by observing shear stresses around the stenosis. Shear stresses are picked up with ultrasound devices. In this thesis, the normal stresses occurring around the stenosis is considered. The radial stresses were related to distances upstream and downstream from the stenosis, similarly to the studies mentioned above. The degree of radial stresses occurring along various distances from stenosis were related and confirmed by two devices, an optical sensor and a piezoelectric vibration sensor. The RPR-220 optical sensor (Rhom Semiconductor) is a sensitive device that measures distance from the sensor by the amount of reflected infrared light intensity. This device was able to measure the distances from the vessel wall to the

sensor, and thus measured the amount of wall deflection occurring upstream, downstream, and on the throat of the stenosis. As shown in figure 24, both models show the least amount of wall deflection over the throat of the stenosis, which corresponds to less normal stresses on the walls in the diseased section. Since the RM has symmetrical rigidity along the diseased section, the walls cannot deflect and therefore, the stresses in that section remain steady and at equilibrium. The LPDM, still has a flexible portion of the wall across the rigid section of the disease. This allows the walls to deflect. The greater wall deflection occurring in the walls upstream and downstream from the stenosis of the LPDM when compared to the RM, shows that resistance along the circumference of the diseased portion dampens wall motion. The experimental setup shown in figure 27 reveals a decrease in wall deflection magnitude with further distance from stenosis shown in figure 28. This implies that the two highest points of deflection occur upstream and downstream from the stenosis. Since the wall motion is reduced in the diseased region, the most energy of wall movement is distributed along the ends of the stenosis. The two highest points of wall deflection detected in a diseased vessel screening through a device such as a piezoelectric material or optical sensor will indicate stenosis. Another relationship with location of stenosis is the frequencies of the wall movement. It was found that the highest frequencies occur in the upstream and downstream locations close to the stenosis. Figure 29 shows as the distance from the stenosis increases, lower frequencies become prominent in the signal. This is another indication of wall movement energy distribution.

The normal stresses occurring on the walls of the vessels as a function of wall deflection has shown to indicate and classify the presence of stenosis. The magnitude

and frequencies of wall displacements have shown to locate the stenosis. These are valuable relationships that can be applied to noninvasive sensors to more accurately detect atherosclerosis.

The greater wall deflection around the stenosis in the LPDM was also confirmed with a piezoelectric material. Figure 24 compares the amount of wall deflection occurring upstream from the stenosis for both LPDM and RM with increasing flow rates. Increasing the flow rates in this experiment does not only show that it causes the walls to deflect more, but it simulates a cardiac cycle. Since we did not use pulsatile flow in the experiments, the higher flow rates examines the condition of peak pulse flow. Other studies working with pulsatile flow, have shown that the magnitude of the results depends on the volumetric flow rates [20], [24], [25]. In this study, the flow passing through the lumen of the vessel and leaving the vessel is an example of an open system. Although blood circulation is part of a closed system, which keeps the vessel pressurized, increasing the flow rates represents circulatory peak flow conditions. Since the diseased vessel models in the experiments are part of an open system, the magnitude of vessel wall pressures are reduced and higher flow rates accommodate the models to closed system conditions.

The FFTs of the stethoscope showed resonance at frequencies such as 60 Hz and other harmonics of 60 Hz, such as 30 Hz, and 120 Hz. Therefore, it is expected that the stethoscope contributes to the sound spectral response of the models. However, the CWTs of the stethoscope signals did show some main differences between the frequency ranges that were also observed in the FFTs of the plethysmography in figure 21. The CWTs in figure 25 show that there is a broader range of frequencies occurring in the

LPDM but more concentrated frequencies in the RM. The signals between the plethysmography and stethoscope could not be correlated because the frequencies do not fall within the same frequency range. The stethoscope sounds are present in higher frequencies. However, the total energy of the dominant frequencies occurring in time can be compared by the CWTs. The CWTs of the plethysmography show for both frequency ranges shown in figures 22 and 23, that there is more energy of wavelet coefficients occurring in time for the SPDM. This relationship between more energy of wavelet coefficients occurring per time was also observed with the stethoscope. It can be observed from figure 25 that there are more periods between frequencies showing up in the RM, thus contributing to less energy of wavelet coefficients per duration of time. This simply means that the vibrations and sounds produced for the SPDM are more constant throughout time. Figure 25 also shows that the sounds in the SPDM vary more in amplitude in time, whereas in the RM, the sounds decrease in amplitude in time. This shows that the sounds of SPDM are more chaotic and represent a nonlinear system. For example, this behavior is known as bursting. An example of what is occurring in the signals is illustrated in figure 39 and 40. Figure 39 shows an example of a signal that has longer periods between signals and decreases over time with their corresponding CWTs. This signal was produced to model and explain further the signal found in the RM shown in figure 25. Similarly, the sounds of the SPDM were modeled to show the unsteadiness in amplitude of sounds, shorter periods between sounds, and longer duration of sounds. The findings in the sounds produced in the SPDM are similar to the results observed by Dr. Tavel in ultrasound data of patients with severe stenosis. Dr. Tavel found that patients with a greater degree of stenosis showed sounds with a longer duration of time

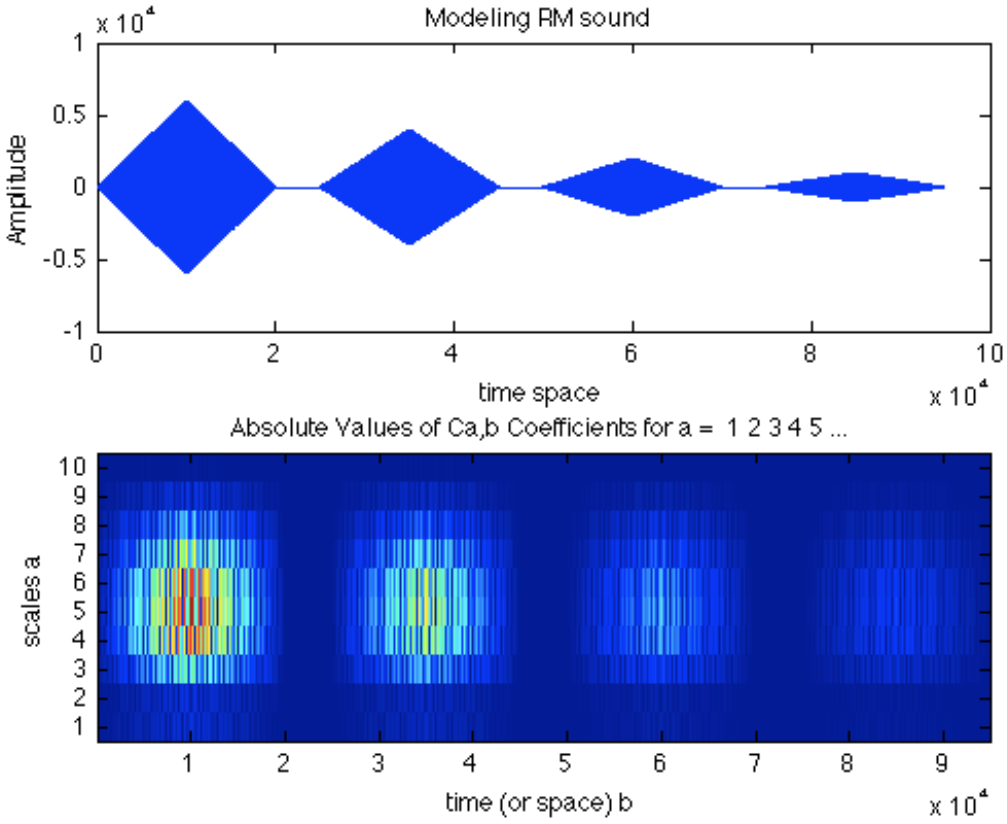

Figure 39: Modeling sounds produced by RM. (Top) Signal (Bottom) CW

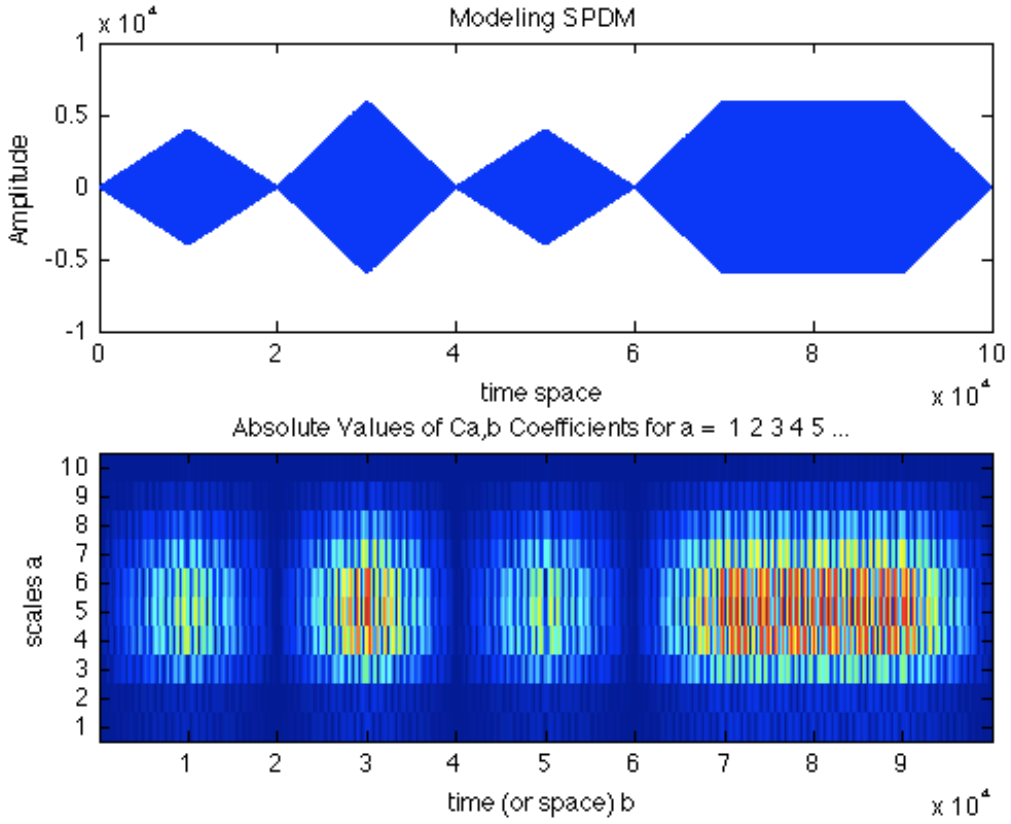

Figure 40: Modeling sounds produced by SPDM. (Top) Signal (Bottom) CWT

and higher frequencies [6]. Although a greater degree of stenosis corresponds to later stages of the disease, the SPDM matches the results found in clinical data. This just means that the SPDM more accurately represents an occluded artery. Symmetrical rigidity occurs in the very late stages of the disease and perhaps clinical data relating to severely diseased growth arteries are not available do to flow reduction.

The vibrations produced in the LPDM are also consistent with results found in clinical data. In this research, the effects of a longer length of stenosis were observed. Figure 30 shows a frequency shift occurring when the length of the stenosis is increased. Therefore, a longer stenosis causes higher frequency vibrations. These results are also similar to the clinical results found by Sikdar et al [34]. Sikdar et al found that a greater degree of stenosis produced higher frequency vibrations. Although the RM shows damping of vibrations, the images of stenosis shown in Sikdar et al is similar to the geometry of the plaque dome models. The data of Sikdar et al also measures a stenosis increasing on one side of the wall, instead of a symmetrical stenosis like the RM. This geometry can be observed from the images illustrated in figure 41.

To observe where the vibrations are coming from, the diseased vessel models were placed with the stenosis closer to the pressure sensor. Since the pressure sensor hose barbs is rigid and reduces in cross-sectional area to fit into the diseased vessel models, the pressure sensor models a stenosis. It was found that the pressure sensor recorded 80 Hz and the 80 Hz became more dominant with increasing flow rates. The LPDM also vibrated at 80 Hz, but the RM did not. This shows that the pressure sensor produced turbulence at 80 Hz, and this turbulence caused the wall vibrations in the

LPDM. However, the symmetrical rigid diseased section in the RM, dampened the wall motion and did not vibrate at 80 Hz. These results are observed in figures 33-36.

Since the RM dampens wall motion, the wall deflections are not correlated much with the pressure sensor. Figure 32 shows that the wall deflections from the LPDM is more correlated with the pressure sensor than RM, and at certain time lags, they are correlated about three times as much. Figure 36 shows that the wall deflections and the turbulence from the pressure sensor have a squared relationship.

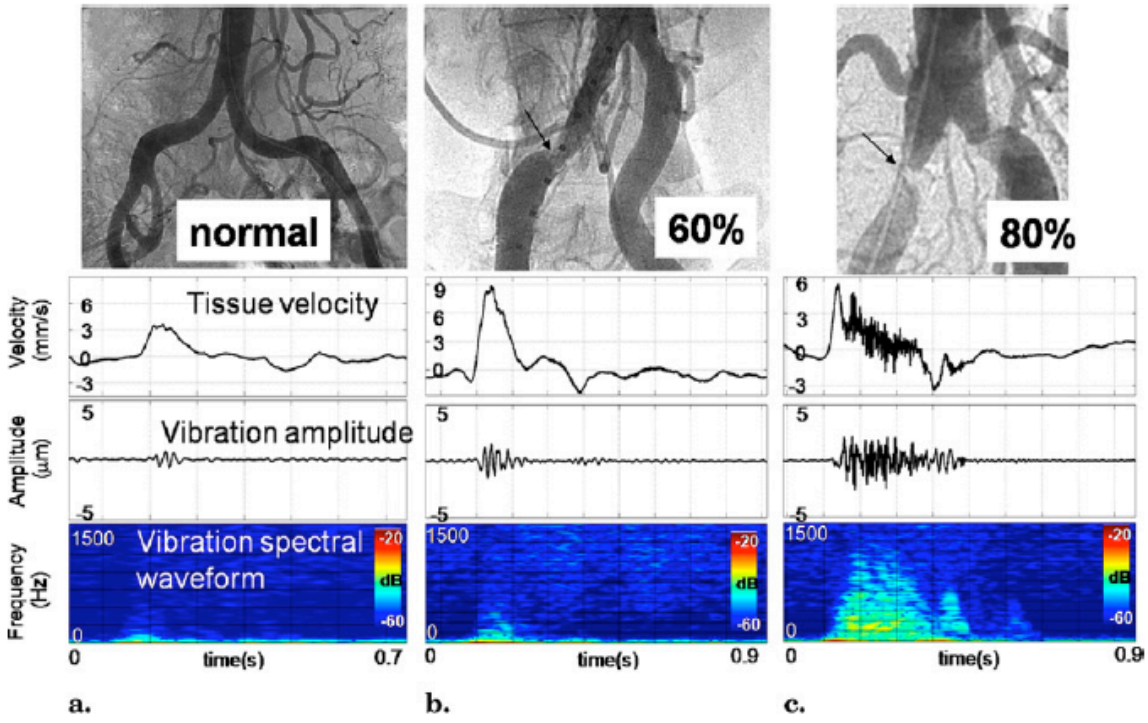

Figure 41: Clinical data by Sikdar et al. [34] showing greater vibrations and for longer duration of time with increased severity.

Chapter 5

Conclusion

It was found that a plaque dome model on one side of a vessel causes the vessel to vibrate. The amount of vibration was related to the length of the stenosis. The plaque dome models showed vibrations within a higher frequency range when compared to the rigid model. When the length of the stenosis was increased in the plaque dome model, higher frequencies were produced. The frequencies present in the plaque dome models were more constant throughout time, a phenomena known as bursting, whereas the frequencies in the rigid model showed to decay quickly over time.

It was found that symmetrical rigidity dampens vibrations and also reduces the amount of wall deflection. The walls deflected on average approximately twice as much upstream and downstream from the stenosis in the long plaque dome model. These intensities in wall deflection across the stenosis can be used to determine location of stenosis. The relationship between wall magnitudes was confirmed using a piezoelectric material and an optical sensor. Another relationship observed was between the frequencies and distance away from the stenosis. It was found that lower frequencies become prominent as the distance upstream from the stenosis increases. This was observed with the plaque dome and rigid geometries. The rigid model's frequencies were more concentrated, even as the distances upstream from the stenosis increased. These findings indicate that a device that can sense wall deflection and vibrations can be used to screen along a length of an artery to sense changes in frequencies and magnitude to reveal location and severity of stenosis.

Since vascular disease continually varies, the models predicted here may be applied to other mechanics and geometries. The results from this study indicate that the plaque dome models agree with similar findings in clinical data [6], [34]. The rigid model has not shown similar results to other clinical studies, possibly because it represents very late stages of the disease. It may however, help explain different cases of stenosis and why bruits are often missed.

The vascular disease models presented in this thesis has been shown to provide a useful approach to the study of the fluid dynamics of vascular disease. This modeling approach has been shown here to provide stable results as opposed to other experimental models that deteriorate rapidly. Moreover, the physical models provided here relieve the assumptions necessary to perform a computational approach to the problem. This study found different relationships that can help locate and detect stenosis severity, which can be implemented with new technologies for general screening of stenosis in order to decrease the number of severity cases and Transient Ischemic Attacks.

REFERENCES

[1] E.V. Limbergen, R. Potter, "Endovascular Brachytherapy," in The GEC ESTRO Handbook of Brachytherapy, pp. 635-637, 2002.

[2] P. Libby, "Inflammation in atherosclerosis", in insight review articles pp.868-874, Nature Publishing Group, 2002.

[3] S. Sen and S. Chakravarty, "Dynamic response of wall shear stress on the stenosed artery," in Computer Methods in Biomechanics and Biomedical Engineering, vol. 12, No. 5, Taylor & Francis Group, October 2009, pp. 523-529.

[4] W.A. Riley, R.W. Barnes, G.W. Evans, G.L. Burke, "Ultrasonic Measurement of the Elastic Modulus of the Common Carotid Artery-The Atherosclerosis Risk in Communities Study," in Stroke, vol. 23, American Heart Association, 1992, pp. 952-956.

[5] R.E Klabunde, "Determinants of Resistance to Flow (Poiseille's Equation)," in CV Physiology, 2010.

[6] M.E. Tavel, J.R. Bates "The Cervical Bruit: Sound Spectral Analysis Related to Severity of Carotid Arterial Disease," in Clinical Cardiology, vol. 29, pp. 462-465, July 2006.

[7] S.K. Samijo, J.M. Willigers, R. Barkhuysen, P.J.E.H.M. Kitslaar, R.S.Reneman, et al., "Wall shear stress in the human common carotid artery as function of age and gender," in Cardiovascular Research, vol. 39, pp. 515-522, 1998.

[8] C.A. Pickett, J.L. Jackson, B.A. Hemann, J.E. Atwood, "Carotid Bruits and Cerebrovascular Disease Risk A Meta-Analysis," in Stroke, vol. 41, American Heart Assosication, 2010, pp.2295-2302.

[9] M.T. Magyar, E.M. Nam, L. Csiba, M.A. Ritter, E.B. Ringelstein, et al., "Carotid artery auscultation—anachronism or useful screening procedure?" in Neurological Research, vol. 24(7), October 2002, pp. 705-708.

[10] J.A. Gift. "Carotid Collar: A Device for Auscultory Detection of Carotid Artery Stenosis," Masters Thesis, Massachusetts Institute of Technology, September 2003

[11] S.O. Oktar, C. Yucel, et al., "Blood-Flow Volume Quantification in Internal Carotid and Vertebral Arteries: Comparison of 3 Different Ultrasound Techniques with Phase-Contrast MR Imaging," in American Journal of Neuroradiology, vol. 27, July 2005, pp. 363-369

[12] B. Belay, P. Belamarich, A.D. Racine, "Pediatric Precursors of Adult Atherosclerosis," in Cardiovascular Disease, Vol. 25, No. 1, pp. 4-13, January 2004

[13] V.P. Eroschenko, "Atlas of Histology with Functional Correlations," 11th edition, Lippincott Williams & Wilkins, 2008, Ch. 8, pp. 174

[14] J. Bakosi, "PDF Modelling of Turbulent Flows on Unstructured Grids," Ph.D Dissertation, George Masson University, April 2008

[15] V.L. Rogers, A.S. Go, D.M. Lloyd-Jones, R.J. Adams, J.D. Berry, T.M. Brown, et.al, "Heart Disease and Stroke Statistics—2011 Update: A Report from the American Heart Association," in Circulation, 123:e18-e209, 2011

[16] B.L. Mintz, R.W. Hobson, "Diagnosis and treatment of carotid artery stenosis," in JAOA, vol. 100, no.11, pp-S22-S26, November 2000

[17] "Carotid Artery Disease," from Vascular Disease Foundation, in http://www.vdf.org/pdfs/VDFOnePage_Carotid.pdf

[18] A.S. Trucksass, D. Grathwohl, A. Schmid, R. Boragk, et al. "Functional, and Hemodynamic Changes of the Common Carotid Artery with Age in Male Subjects," in Arteriosclerosis, Thrombosis, and Vascular Biology- Journal of the American Heart Association, 19;1091-1097, 1999

[19] L. Ai, L. Zhang, W. Dai, C. Hu, K.K. Shung, T.K. Hsiai, "Real-time assessment of flow reversal in an eccentric arterial stenotic model," in Journal of Biomechanics, vol. 43, pp. 2678-2683, 2010

[20] B. Wiwatanapataphee, "Modelling of Non-Newtonian Blood Flow Through Stenosed Coronary Arteries," in Dynamics of Continuous, Discrete and Impulsive Systems Series B: Applications & Algorithms, vol. 15, pp. 619-634, 2008

[21] J.S. Milner, J.A. Moore, B.K. Rutt, D.A. Steinman, "Hemodynamics of human carotid artery bifurcations: Computational studies with model reconstructed from magnetic resonance imaging of normal subjects," in Journal of Vascular Surgery, vol. 27, pp. 143-156, 1998

[22] H. Huang, V.J. Modi, B.R. Seymour, "Fluid Mechanics of Stenosed Arteries," in International Journal of Engineering Science, vol. 33, no. 6, pp. 815-828, 1995

[23] J.H. Choi, N.L. Kang, S.D. Choi, "Understanding of Navier-Stokes Equations via a Model for Blood Flow," in Journal of the Korean Society For Industrial and Applied Mathematics, vol. 11, no. 1, pp. 31-39, 2007

[24] A. Valencia, F. Baeza, "Numerical simulation of fluid-structure interaction in stenotic arteries considering two layer nonlinear anisotropic structural model," in International Communications in Heat and Mass Transfer, vol. 36, pp. 137-142, 2009

[25] A. Valencia, M. Villanueva, "Unsteady flow and mass transfer in models of stenotic arteries considering fluid-structure interaction," in International Communications in Heat and Mass Transfer, vol. 33, pp. 966-975, 2006

[26] Q. Lu, M. Arroyo, R. Huang, "Elastic Bending Modulus of Monolater Graphene," in Journal of Physics D: Applied Physics, vol. 42, 2009, pp. 102002

[27] G.M. Drzewiecki, J.K. Li, A. Noordergraaf, "Modeling Vascular Vibrations: Autoregulation and Vascular Sounds," in The Biomedical Engineering Handbook, ed. Bronzino, CRC press, in press.

[28] B.J. TenVoorde, Th.J.C. Faes, O. Rompelman, "Spectra of data sampled at frequency-modulated rates in application to cardiovascular signals: Part1 analytical derivation of the spectra," in Medical and Biological Engineering and Computing, vol. 32, no. 1, 1994, pp. 63-70

[29] D. Tang, C. Yang, H. Walker, S. Kobayashi, D.N. Ku, "Simulating cyclic artery compression using a 3D unsteady model with fluid-structure interactions," in Computers and Structures, vol. 80, pp. 1651-1665, 2002

[30] D.S. Sankar, A. Izani, "Two-Fluid Mathematical Models for Blood Flow in Stenosed Arteries: A Comparative Study," in Boundar Value Problems Hindawi Publishing Corporation, 2009

[31] U.A. Bakshi, V.U. Bakshi, "Basics of Electrical Engineering," First Ed. Technical Publications Pune, 2008

[32] J.D. Cutnell, K.W. Johnson, "Physics," 4th ed. New York: Wiley, 1998, pp. 466

[33] S. Kim, "A Study of Non-Newtonian Viscosity and Yield Stress of Blood in a Scanning Capillary-Tube Rheometer," Doctor of Philosophy Thesis, Drexel University, December 2002

[34] S. Sikdar, "Doppler Vibrometry: Assessment of Arterial Stenosis by Using Perivascular Tissue Vibrations without Lumen Visualization," 2009, in press

[35] A. Miller, R.S. Lees, J.P. Kistler, W.M. Abbott, "Effects of surrounding tissue on the sound spectrum of arterial bruits in vivo," in Stroke, Journal of the American Heart Association, 1980, 11:394-398

[36] A.S. Turak, K.M. Johnson, D. Lum, et al, "Physiologic and Anatomic Assessment of a Canine Carotid Artery Stenosis Model Utilizing Phase Contrast with Vastly Undersampled Isotropic Projection Imaging," in American Journal of Neuroradiology, January 2007, 28: 111-115